Development and characterization of paired *in vivo* and *in vitro* models to examine obesity-linked colorectal cancer

by

Bulbul Ahmed

A dissertation submitted to the Graduate Faculty of
Auburn University
in partial fulfillment of the
requirements for the Degree of
Doctor of Philosophy

Auburn, Alabama
December 14, 2019

Keywords: Colorectal cancer, Patient derived xenograft, 3D engineered CRC tissue, adipose tissue, high-fat Western diet, RNA-sequencing

Approved by

Michael W. Greene, Chair, Associate Professor, Nutrition, Dietetics and Hospitality Management
Kevin W. Huggins, Associate Professor, Nutrition, Dietetics and Hospitality Management
Ramesh B. Jeganathan, Associate Professor, Nutrition, Dietetics and Hospitality Management
Elizabeth Lipke, Associate Professor, Chemical Engineering

Abstract

Currently, obesity has become a global issue and is referred to as an epidemic. Contemporarily, colorectal cancer (CRC) is the fourth most common cause of cancer-associated death worldwide. Several epidemiological studies demonstrated that obesity is linked to CRC. Obesity is characterized as a chronic low-grade inflammation which is assumed to be a crucial risk factor for CRC. However, the mechanism behind obesity-associated CRC is elusive. To investigate the link between obesity and CRC, and to develop a platform to screen and test therapeutic agents targeting CRC in the obese state, our objectives were to develop an innovative experimental model of obese insulin resistance *in vitro* which can facilitate the *in vivo* obese insulin resistance adipose tissues and also to develop a new obesity-linked engineered 3D cancer co-culture system that may serve as a platform to screen therapeutic agents against obesity-linked CRC.

 To develop an obese insulin resistance model *in vitro,* differentiated 3T3-L1 adipocytes were treated with Tumor Necrosis Factor alpha (TNF-α) and hypoxia for 24 hours, and then, extra glucose and Fetal Bovine Serum (FBS) were added for 72 hours. TNF-α and hypoxia significantly reduced expression of insulin-sensitive genes and induced expression of insulin resistant genes. Adipocytes lost lipid content over time and the insulin-stimulated AKT phosphorylation significantly decreased. This result indicates that combined TNF-α and hypoxia have the potential to induce long-term an obese insulin resistance phenotype *in vitro*.

 To investigate CRC *in vivo*, we developed a standardized platform for obesity-linked CRC study *in vivo* using PDX CRC tumors implanted orthotopically. PDX CRC tumors were implanted in the diet-induced obese Rag1 (B6.129S7-*Rag1^{tm1Mom}*/J) mice. Diet-induced obese Rag1 mice developed insulin resistance, which promoted tumor growth.

To establish a unique *in vitro* platform, we fabricated 3D engineered CRC tissues. Three lines of tumors were obtained from three different patients, and tumors were propagated in SCID (NOD.Cg-*Prkdc*^scid Il2rg^tm1Wjl/SzJ) mice subcutaneously for 29 days. Cells from the PDX tumors were also encapsulated and propagated in Poly (ethylene glycol)-fibrinogen (PEG-Fb) hydrogel to form a 3D tissue, which we define 3D engineered CRC tissue. The results showed that the phenotype of the growth of 3D engineered CRC tissues followed the growth of the *in vivo* tumors. We also examined the 3D engineered CRC tissues grown by co-culturing with the long-term insulin resistant adipocytes. The *in vitro* 3D tissues were enabled to recapitulate the *in vivo* microenvironment, and most prominently the obese insulin resistant adipocytes were able to enhance of the growth of the 3D engineered CRC tissues. Finally, we performed mRNA sequencing of PDX CRC tumors propagated in SCID mice and 3D engineered CRC tissues. Interestingly, the sequencing data demonstrated that the gene expression characteristics of PDX CRC tumors propagated in SCID mice clustered with the 3D engineered CRC tissues, indicating that each PDX line has a unique gene expression profile.

Overall, our study observed that the 3D engineered CRC tissue scaffold facilitates the *in vivo* tumor microenvironment similar to the tumor propagated in SCID. The co-culture study has demonstrated that the insulin resistant adipocyte model can lead to enhanced 3D engineered CRC tissue growth, which may serve as a platform for further research on obesity-linked CRC study.

Dedication

I would like to dedicate this dissertation to the people who are making this world livable by their

honesty and hard work.

Acknowledgment

I would like to thank Dr. Michael W. Greene for allowing me into his lab and serving as my dissertation mentor. Dr. Greene has been an enthusiastic mentor throughout my entire graduate program. I also like to thank Dr. Kevin Huggins, Dr. Ramesh Jeganathan, and Dr. Elizabeth Lipke for serving as my dissertation committee and for their guidance in my research. I express my gratitude to Dr. Ann Marie O'Neill for her guidance and help in experiment preparation.

Especially thanks to my colleagues Ms. Lauren Woodie, Dr. Yuwen Luo, Mr. Peyton Kuhlers, Dr. Vishal Kothari, Dr. Chen Zheng, Dr. Yueru Li, Ms. Marina Sycheva, Ms. Yuxuan Zhang, Ms. Yijing Qi, Ms. Olivia Atonji, Ms. Priscilla Ayine, Dr. Vaithinathan Selvaraju, and Dr. Shraddha Rege for their support and friendly attitude in my PhD work. It was a great pleasure to study and to work together.

I express my sincere gratitude to all faculty members in the Department of Nutrition, Dietetics and Hospitality Management, and the College of Veterinary Medicine at Auburn University for giving me an opportunity and atmosphere to conduct my research.

I would like to thank my wife for her patience and inspiration, and thanks to my daughter Junahnai who teaches me what love is. Deepest thanks to my parents for their enormous support and hardship for growing me up to here. Also, thanks to the Auburn University Research Initiative in Cancer (AURIC) for funding support.

Table of Contents

List of Tables

List of Figures

Abbreviations

Colorectal cancer (CRC)

Poly (ethylene glycol)-fibrinogen (PEG-Fb)

Body mass index (BMI)

Free fatty acids (FFAs)

Monocyte chemotactic protein-1 (MCP-1),

Glucose transporter type 4 (GLUT4)

C-C Motif Chemokine Ligand 2 (CCL2)

Solute Carrier Family 2 Member 4 (slc2a4)

Eukaryotic Translation Elongation Factor 2 (eef2)

Tumor necrosis factor (TNF-α)

Interleukin 1 beta (IL-1β)

Interleukin (IL-6),

Glyceraldehyde-3-Phosphate Dehydrogenase (GAPDH)

Toll-like receptors (TLRs)

Adipose tissue macrophages (ATMs)

Crown-like structure (CLS)

Reactive oxygen species (ROS)

Superoxide ($^{\bullet}O_2^-$),

 Hydrogen peroxide (H_2O_2),

Hydroxyl radical ($^{\bullet}OH$), and

 NADPH oxidase (NOX)

Oxidative stress (OS)

Endoplasmic reticulum (ER)

Phosphatidylcholine (PC)

Phosphatidylethanolamine (PE)

C/EBP homologous protein (CHOP)

Unfolded protein response (UPR)

PKR like ER kinase (PERK),

Inositol requiring enzyme 1 (IRE1), and

Activating transcription factor 6 (ATF)

Mammalian Target of Rapamycin (mTOR)

AMP-dependent protein kinase (AMPK)

S-nitrosoglutathione reductase (GSNOR)

Consensus molecular subtypes (CMSs)

Chromosomal instability (MSI)

Copy number alterations (SCNA)

Dulbecco's modified Eagle's medium (DMEM)

Glutamine, and penicillin-streptomycin (p/s)

Phosphate-buffered saline (PBS)

Tris-buffered saline with 0.1% Tween20 (TBST)

Quantitative polymerase chain reaction (qPCR)

Reverse transcriptase Quantitative polymerase chain reaction (RT-qPCR)

Patient-derived xenograft (PDX)

Nnuclear factor kappa-light-chain-enhancer of activated B cells (NF-κB)

NOD-SCID gamma (SCID)

Endothelial to mesenchymal transition (EMT)

Beta-2-Microglobulin (B2M)

Transforming growth factor beta 1 (TGF-β1)

Snail Family Transcriptional Repressor 1 (SNAI1)

Twist Family BHLH Transcription Factor 1 (TWIST1)

Aldehyde Dehydrogenase 1 Family Member A1 (ALDH1A1)

Glutathione Peroxidase 2 (GPX2)

Leucine Rich Repeat Containing G Protein-Coupled Receptor 5 (LGR5)

Olfactomedin 4 (OLFM4)

Kinase Insert Domain Receptor (KDR)

Vascular Endothelial Growth Factor A (VEGFA)

Fibrinogen (PF)

Poly (ethylene glycol) diacrylate (PEGDA)

Epididymal white adipose tissue (EWAT)

Homeostatic Model Assessment of Insulin Resistance (HOMA-IR)

High Fat Diet (HFD)

Rag1tm1Mom (Rag1)

High fat diet with sugar water (HFS)

Enzyme-linked immunosorbent assay (ELISA)

Analysis of variance (ANOVA)

Messenger RNA (mRNA)

Chapter 1: Introduction

Obesity has become an epidemic worldwide and it is an important public health concern. In the US, almost 40% of adults are considered to be obese [2] and it is the second most preventable cause of death [3]. Obesity has nearly tripled since 1975, and it is estimated that 51% of the population will be obese by 2030 [4]. During chronic over nutrition, the excess nutrients are stored as lipid in adipose depots causing obesity. In prolonged over nutrition, the excess free fatty acids stored in different organs as ectopic fat produce inflammation. Obesity-induced inflammation contributes a pivotal role in the development of insulin resistance, which is a risk factor for many chronic diseases such as cancer, type 2 diabetes, hypertension, atherosclerosis, and cardiovascular diseases [5].

There is a strong link between obesity and colorectal cancer (CRC) [6-8]. CRC is the third most common cancer diagnosed and fourth-most common cancer-associated death worldwide, which is about 1.4 million new cancer cases and almost 70 thousand deaths [9]. CRC is the costliest type of cancer and the estimated indirect and direct cost will be $ 17 billion by 2020 [10]. The five year survival rate is 65% after being diagnosed [11]. High incidence areas for CRC are in the United States, Europe, and Oceania [12]; it is believed that increasing adaptation to a Western life, including high sugary water, high saturated fat, and high-energy dense food consumption, are the leading causes.

Epidemiological evidence has linked diet-induced obesity and abdominal fat with an increased the risk of CRC [13]. In the obese condition, cytokines and growth factors released by adipose tissues have tumorigenic effects in the gastrointestinal tract, which promote CRC [14]. Several studies have shown that diet-induced obese insulin-resistant mice develop pro-inflammatory environments, which are

associated with increased proliferation and decreased apoptosis of CRC tumor cells [15-18]. However, the complete understanding of the pathophysiology of obese insulin-resistant states linked CRC is elusive.

Our goal, in this study, is to examine the role of obese insulin resistance that promotes CRC tumor growth. Therefore, the mechanism by which obesity and its associated pathophysiology promoting CRC growth can be identified. In our first aim: the potency of TNF-α and hypoxia to induce insulin resistance in the differentiated 3T3-L1 adipocytes has been examined to establish a long-term *in vitro* obese insulin resistance model. In our second aim: the growth, morphology and gene expression of 3D engineered CRC tissues in the poly(ethylene glycol)-fibrinogen (PEG-Fb) has been demonstrated, and the 3D engineered CRC tissue has been co-cultured with the long-term obese insulin resistance model to characterize the growth of 3D engineered CRC tissue. In our third aim: an orthotopic PDX CRC animal model has been established to serve as an *in vivo* platform to pair with *in vitro*.

Chapter 2: Literature review

2.1 Obesity

2.1.1 Definition of obesity

Obesity is a medical condition in which excess body fat has accumulated to the extent that it may have an adverse health effect. Obesity is defined by the National Institute of Health on body mass index (BMI), which is measured by the person's weight in kilograms divided by the square of height in meters. If the BMI is above 30, the individual is considered to be obese. The enlargement of fat mass characterizes obesity through adipocyte cell size increase (hypertrophy) and proliferation (hyperplasia) [19]. The excess accumulation of body fat is usually caused by the consumption of more macronutrients than the body requires. This excess nutrition is then stores as triglyceride, which is commonly known as a fat, and adipocyte cells that stored triglyceride are known as fat cells. The primary composition of the adipose tissue is adipocyte cells. Adipose tissue is a large and dynamic endocrine organ responsible for energy storage, making up between the range from 2–3% of body weight and 60–70% of body weight in humans [20]. When adipocytes cannot uptake more triglycerides, the body synthesizes new adipocytes which creates enormous space for fat storage [21]. The adipose tissues are distributed in several areas in the human body, such as visceral, epicardial, perirenal, craniofacial, gonadal, intramuscular, marrow, ectopic, subcutaneous, etc. During the consumption of excess nutrition, the fat tends to accumulate in the visceral and subcutaneous depots and make these depots bigger by hypertrophy and hyperplasia. Evidence has shown that unhealthy obesity is associated with adipose tissue precursor that restricts to hyperplastic remolding of expansion, leading to adipocytes hypertrophy and systemic metabolic dysfunction [22]. Hypertrophic obesity is associated with abdominal obesity, which recruits macrophages, promotes local inflammation, and accumulates ectopic fat [23, 24].

Approximately 10-25% of obese individuals are metabolically healthy [25] because their insulin is sensitive and is not prone to develop any associated diseases. However, a recent study has shown that metabolically healthy obesity is not a harmless condition, who remain free of metabolic diseases for decades face an increased risk of cardiovascular events [26]. The rest of the metabolically unhealthy obese individuals are characterized by bigger visceral fat mass and lower subcutaneous fat mass. The impaired fat storage capacity of the adipose tissue may result in ectopic fat deposition and contributing to developing insulin resistance [27]. Unhealthy obesity is associated with several chronic conditions directly, such as kidney diseases, osteoarthritis, cancer, diabetes, sleep apnea, nonalcoholic fatty liver disease, hypertension, and cardiovascular diseases [28].

2.1.2 Prevalence and incidence

Obesity rates are increasing frighteningly worldwide; since 1975, obesity nearly tripled. A study found that between 1975 and 2014, the prevalence of obesity increased from 3.2 to 10.8% in men and 6.4 to 14.9% in women in a standardized age. If the trend continues, 57.8% of the world population will be overweight or obese by the year 2030 [29]. A total of 1.9 billion adults aged 18 and over were overweight, and 650 million of them were obese, which is 13% of the total population. Prevalence of obesity among children and adolescents aged 5-19 is also high; about 340 million children and adolescents were overweight or obese in 2016 worldwide [30]. More specifically, the prevalence of obesity among US, adults were 39.8%, and among them, 36.6% were men, and 41% were women. The prevalence of obesity was higher among 40-59 years of age (42.8%) in 2016 [31]. Hispanics and non-Hispanic blacks had the highest age-adjusted prevalence of obesity in the US, followed by non-Hispanic whites and non-Hispanic Asians. The estimated total annual health care cost of obesity was 147 billion dollars, and the medical cost for people who had obesity was $1,429 higher than those of normal

weight[32]. In 1990, obese adults made up less than 15% of the population in most states in the US [33]. By 2010, 36 states had obesity rates 25% or higher, and 12 of those had obesity rates of 30% or higher [34]. Currently, nationwide, approximately two out of three US adults are overweight or obese, and one out of three (40%) are obese [31]. Obesity is also rising among children and adolescents alarmingly, one out of 5 children and adolescents ages 2 to 19 are obese [31]. Early obesity does not only increase the likelihood of adult obesity, but it also increases the risk of several diseases.

2.1.3 Risk factors

There are many risk factors for obesity. Some risk factors depend upon the environment and lifestyle, and some are independent. Regardless of the environment, independent risk factors are modifiable and change themselves systematically. Here are some explanations of independent and dependent risk factors for obesity.

2.1.3.1 Environmental factors: Environmental factors increase the risk of becoming overweight and obese. Nowadays, the community is structured in such a way that it may contribute to obesity. High energy condensed foods are very accessible and cheap in the community. Unhealthy foods now sell in places like gas stations and office supply stores, which were never seen historically. The processed, high energy condensed food products are intensively marketed on televisions and radios. Because of the availability of these foods, the people of lower socioeconomic status have frequent access to these foods that cause obesity.

Limited access to physical activity or recreational facilities is also variably associated with increasing obesity [35]. Physical activity or recreation of neighborhood spaces has been associated with increased

physical activity and a healthy food environment. A landmark study on the spread of obesity for a 32 years prospective data found that an individual's chances of becoming obese increased by 57% if he or she had a friend who became obese in a given 4-year interval [36]. The same study has also showed that persons of the same sex have a relatively greater influence on each other than those of the opposite sex [36]..

Environmental temperature is also a concern for obesity, when the ambient temperature increases or decreases, energy expenditure also increases or decreases to maintain human body homeostasis [37]. Humans have an optimal body temperature, which is higher than the temperature of the environment. In the cooler temperature, the human body adjusts its temperature by increasing metabolic rates. The metabolic rate also increases when the ambient temperature rises. With the widespread control of climate by heating and air conditioning in cars, homes, and workplaces, humans enjoy comfortable temperatures where energy demands are minimized. Because of more time spent in this thermoneutral zone, it may associate with increasing obesity [37].

2.1.3.2 Genetics: Genetics is also a strong risk factor for obesity. Genes may affect the amount of body fat stored and distributed. Genes also affect how efficiently the body uses food for energy. Diet, lifestyle, and other exposure influence to modify or methylate genes that have been implicated in subsequent offspring, which increased risk for obesity, including famine exposure, parental obesity, smoking, endocrine-disruption, and other chemicals, as well as weight gain during gestation and gestational diabetes [38]. Genetic modification also depends upon the food habits during pregnancy, which can change the baby's DNA by methylation, which may affect on child's fat deposition [39]. Obese fathers also have DNA methylation at imprinted genes in human sperm that may pass on to their children [40].

There are a number of genes that may contribute to obesity; however, only 32 of the most common genes are thought to be responsible for the overall variation in obesity [41].

2.1.3.3 Aging: Aging is associated with changes in body composition. The total fat mass rearranges in the aging process, such as increases the ectopic fat depositions in the liver and skeletal muscle, and the visceral deposition in the abdomen. Several studies have supported that decreasing energy expenditure plays a critical role in increasing fat deposition in the aging process. After the age of 20, the resting energy expenditure rate decreases by 2-3% per decade and skeletal muscle mass reduces 40% by periods between 20 to 70 years [42]. Additionally, physical activity declines and people become sedentary which may reduce half of the total energy expenditure in old age[42]. Interestingly, the body weight and body fat mass tend to be a maximum at the age of 65 for men and reduce in the following years [43] [44], while for women the body weight increases to its maximum ten years later than the men[44]. In the following years, both for men and women, body fat mass, muscle mass, and free fatty acid tend to decrease. Remarkably, though the body fat mass percentage decreases in old age, the percentage of body fat mass becomes higher in elderly persons compared to young adults [45]. Long-term maintenance of a healthy diet is more effective plan to mitigate weight gain from middle age to old age [46].

2.1.3.4 Gut microbiota: The **g**astrointestinal tract contains a dense amount of microbes such as bacteria, fungi, archaea, and viruses which are collectively called gut microbiota; inside of the human gut contains trillions of microbes more than ten times of total human body cells [47]. The most predominant phyla in the human gut microbiota are *Bacteroidetes* and *Firmicutes*, which are about 90% of human gut microbiota [48]. Gut microbiota are very important for body homeostasis for amino acid metabolism, lipopolysaccharide biosynthesis, RNA degradation, steroid hormone biosynthesis, small chain fatty acid

production, and modulation of the immune system [47, 49]. An individual's gut microbiota composition is influenced by various factors, such as diet, age, birth delivery, breastfeeding, use of antibiotics, ethnicity, host genetics and history of medication[50]. In fact, the intestine of a newborn is not sterile at all; when a baby is in utero, the very first microbiota transfer to infant intestine is from the mother's uterus[51]. The variability starts at the birth of a baby as soon as amniotic fluid disappears; in the case of normal delivery, gut microbiota resembles the vaginal microbiota composition, and in the case of cesarean section, gut microbiota resembles the skin microbiota composition [52].

Diet is the biggest modulator of gut microbiota. Increased intakes of fiber and low caloric diet (plant-based) increase gut microbiota diversity with low microbial gene richness [53] whereas diversity becomes less in case of a high-calorie diet. In obese animals, gut microbiota is more active than lean animals. Obese humans also have a higher amount of small chain fatty acids and reduced amount of caloric content in fecal materials [54]. Therefore, it is assumed that obese individuals intake a higher caloric diet than lean people, and during high caloric diet adaptation, the adapted gut microbiota compositions become more active for energy biosynthesis. A study has shown that transplanting gut microbiota from western diet mice to low-fat plant polysaccharide-rich diet mice increases by 43% the total body fat after two weeks of colonization in the plant diet mice despite the same foods [55]. Similar results were observed when obese human fecal microbiota transferred to mice contributed to fat mass regulation [56, 57]. In the obese individual, a common bacteria family *Firmicutes* is highly increased in gut microbiota. *Firmicutes* are responsible for metabolizing bile acid into active secondary bile acid (deoxycholic or lithocholic acid) which is highly responsible for lipid emulsification and transportation from gut to the liver [50, 58].

2.1.3.5 Diets: The foods and beverages we consume every day have an essential role in our overall health. In the optimal diet, adequate nutrients and energy are required for healthy tissue maintenance and growth. The human body in good health needs the essential nutrients: proteins, carbohydrates, fats, vitamins, and minerals from a wide variety of nutritional foods. Because of urbanization and high income, diets with high sugar, fat, and animal meat replaced traditional diets which are high in carbohydrates and fats [59, 60]. Ethnic and unique, traditional healthy food habits are increasing being replaced by Western high sugar-containing soft drinks, energy-dense fast food, and animal products [60]. The increasing Westernization and mechanical life in the most developed countries is associated with changing in the diet toward high fat, sugar-sweetened beverages, and a sedentary lifestyle [59]. The trend of Westernization is also influencing middle and low-income countries; therefore, obesity and nutrition deficiency are also increasing in low-income countries. Regardless of dietary patterns, evidence from clinical trials has shown that only caloric restriction is associated with weight balance [61].

Overeating sugar, saturated fat, and frequently taking meals have an impact on obesity. The overconsumption of added sugar is one of the most important factors that directly causes long-term development of obesity. Here, the definition of added sugar means all the sugars added to food rather than natural foods, such as glucose, sucrose, maltose, dextrose, and fructose. A study reported that there was a 1.63 to 5.24 lb change in weight within each 4-year period in the three cohorts through the middle age group who were used to consuming sugar-sweetened beverages, potato chips, processed and unprocessed red meats, compared to the group who were used to taking vegetables, fruits, whole grains, nuts, and yogurts [46]. Lack of breastfeeding, high early energy intake, and high intake of sugar-sweetened beverages are also the main contributor to childhood obesity [62]. Consumption of saturated fat was also linked to a higher risk of obesity development. Eating a meal with high saturated fat impacts

insulin sensitivity, increases high postprandial blood sugar and inflammation, contributing to obesity. Dietary fat is much more energy-dense than protein and carbohydrates, but it has less potential to inhibit food intake and evoke insulin secretion [63].

2.1.4 Cellular dysfunction associated with obesity-induced insulin resistance

2.1.4.1 Inflammation: Numerous mechanisms underlie the complication of obesity. Adipocyte cell size increases with weight gain, which elevates adipocyte cell death because of an inadequate supply of oxygen in the face of expanding adipose tissue [64]. The enlarged adipocyte releases more than the usual amount of free fatty acids (FFAs) and pro-inflammatory adipokines such as monocyte chemotactic protein-1 (MCP-1), tumor necrosis factor (TNF-α), Interleukin 1 beta (IL-1β) and interleukin (IL-6), which interact with toll-like receptors (TLRs) of monocytes to attract in the inflammation sites. Once the monocytes join with adipose tissues at the inflammation site, monocytes become mature macrophages [64, 65]. In the obese condition, the phenotypes of resident adipose tissue macrophages (ATMs) polarize from an anti-inflammatory M2 to pro-inflammatory M1. Resident pro-inflammatory M1 macrophages release cytokines, including MCP1 which are able to recruit monocytes, which depend on the adipocyte sizes and conditions. Macrophages and adipocytes interact in a paracrine manner. The macrophages that surround the death adipocytes also make a crown-like structure (CLS) to scavenge the dead cells; the prevalence of CLS is highly interconnected with the metabolic disorder and inflammations [66, 67]. Eventually, together, the ATMs and adipocytes release large amounts of pro-inflammatory proteins that recruit more monocytes; the percentage of ATMs in obese adipose tissue can reach over 50% [68]. Also, the recruited pre-adipocyte progenitors in the adipose tissue become differentiated to mature adipocytes and grow larger in chronic over-nutrition. The size of the adipocytes increases with increases in body fat mass [69]. Dysfunctional adipose tissues induce more inflammations, which

intensify macrophage recruitment, release FFAs, and other pro-inflammations, shortly after released acute FFAs and pro-inflammations start to develop insulin resistant environments.

2.1.4.2 Reactive oxygen species: The risk of obesity is not only dependent on the excess fat stored in adipose depots but also on the fat distribution around different organs. In fact, one study claimed that insulin resistance was not induced by fat accumulation itself in adipose tissues but instead by the inflammation caused by ectopic fat [70]. The chronic overproduction of FFAs in obese conditions leads to storage of fat in muscle, heart, and liver, which are not a safe place for fat storage. Storing excess fat in the wrong places generates lipotoxicity, which produces different lethal reactive oxygen species (ROS) such as superoxide ($^{\bullet}O^{-}_{2}$), hydrogen peroxide (H_2O_2), hydroxyl radical ($^{\bullet}OH$), and NADPH oxidase (NOX). ROS cause dysfunctions in the mitochondria and induce stress in the endoplasmic reticulum. Obesity is characterized by chronically increased oxidative stress (OS) caused by elevated ROS production. Excess production of OS damages cellular structures and functions, leading to the development of obesity-related complications. Obesity induces ROS through multiple biochemical mechanisms such as oxidative phosphorylation, superoxide generation from NOX, glyceraldehyde auto-oxidation, chronic inflammation, protein kinase C activation, and hyper-leptinemia [71]. A study has shown that excess cytosolic fat deposition in the liver, muscle, and pancreatic-β-cells becomes metabolically activated by accompanying long-chain acyl-CoA esters. These esters prevent mitochondrial adenine nucleotide translocations which creates intra-mitochondrial ADP deficiency; therefore, this ADP deficient environment stimulates $^{\bullet}O^{-}_{2}$ radicals in mitochondria [72]. Another study has shown that the conjugated FFAs stimulate the formation of free radicals in adipocytes as well as to induce lipid peroxidation in men with abdominal obesity [73, 74]. In this case, on obese human's lipid peroxidation rate of skeletal muscle becomes 4.2-fold higher than lean humans [75]. Excess FFAs also

stimulate NOX production significantly through the PKC dependent pathway in vascular cells within 72h treatment *in vitro* [76]. Myocardial lipid content also produces a higher rate of superoxide, which develops myocardial oxidative injury in a rat study [77]. *In vitro*, ROS activate potential serine/threonine kinase cascades which interact with several targets in the insulin signaling pathways. One of the important actions of ROS is to regulate the insulin receptor and the family of IRS proteins. ROS activation of serine kinases results in hyper serine/threonine phosphorylation of IRS-1 and IRS-2 which reduces insulin receptor catalyzed tyrosine phosphorylation of IRS-1 and IRS-2 [78]. ROS mediates activation of serine/threonine kinases including: IKKβ, JNK, PKC delta, and P38 MAPK. IKKβ is an important mediators inflammation through the NFκB pathway [78] leading to insulin resistance.

2.1.4.3 Mitochondrial dysfunction: The mitochondria is an essential organelle that generates energy as ATP in a catalytic pathway for the maintenance of normal physiological function. It has dynamic processes to adapt in systematic manner and respond to the metabolic environments such as fusion, fission, biogenesis, and mitophagy. The dysfunction of systemic mitochondrial processes impairs energy production and causes several metabolic alterations as well as damages. Excess consumption of nutrients and obese conditions are associated with mitochondrial dysfunction [79]. There is a possibility to affect mitochondrial dysfunction in all cells; however, in the case of obesity, most mitochondrial dysfunction affects adipose tissues, muscles, and liver, because these organs are involved in high energy processes with an excessive overload of nutrition and FFAs. Studies have shown that the dysfunction of mitochondria in adipocytes of obese human individuals reduces mitochondrial oxidative capacity and biogenesis, which is involved with insulin resistance, metabolic alterations, and low-grade inflammations [80, 81]. In the skeletal muscles, mitochondria become smaller and shorter because of increasing mitochondrial fission in obese mice that reduces mitochondrial function and mass, which is

associated with mitochondrial dysfunctions and insulin resistance [82-84]. Impaired macrophages in skeletal muscle reduce fatty acid oxidation and glucose transportation [85]. It is also reported that mitochondrial fission increases in diet-induced obesity, which decreases respiratory capacity and protein expression in the liver [82]. The characteristics of mitochondria in obese individuals are different compared to lean individuals. In obese individuals, the mitochondria have low energy generation capacities, the internal membrane becomes undefined, fatty acid oxidation decreases, and glucose burden increases, which lower ATP synthesis [79, 85]. The excess ingestion of over nutrition regulates huge mitochondrial dysfunction, which increases mitophagy (the process that removes dysfunctional mitochondria). Mitophagy decreases the numbers of mitochondria, indicating more lipid accumulation. Because of excess lipid and glucose overload, mitochondria produce more than the required amounts of ROS. In healthy mitochondria, less than 5% of collected oxygen produce ROS; in the case of obesity, mitochondria produce uncontrollable ROS, which damages the DNA, lipid membranes, protein and enzymes of the mitochondrial respiratory chain and causes insulin resistance [86]. Excess ROS make oxidative stress and activates numerous transcription factors, including NFκB, which induces elevated circulating and local of pro-inflammatory cytokines to promote an insulin resistant environment [87].

2.1.4.4 Endoplasmic reticulum stress: The endoplasmic reticulum (ER) is another crucial organelle in a eukaryotic cell. The primary functions are protein folding and transportation; ER also maintains Ca^{2+} homeostasis and lipid synthesis [88]. Recently, stress in the ER is highlighted as the key player in the development of obesity associated metabolic dysfunction. During ER stress, lipids and unfolded/ misfolded proteins are accumulated in the ER. Hotamisligil et al. has demonstrated that during chronic over-nutrition and obesity, the liver increases lipogenesis and gluconeogenesis for energy storage, which creates excess lipid overload. Because of excess lipids, ER suppresses protein synthesis and stimulates

lipid biosynthesis. The lipid drops synthesized in the ER by lipogenesis prefer phosphatidylcholine (PC) for a phospholipid coat. In the *de novo* synthesis of fatty acids, the liver produces a massive amount of monounsaturated fatty acids, which is also incorporated into PC. Whereas phosphatidylethanolamine (PE) is another major membrane phospholipid, decreases compared to PC. The PC/PE ratio impaires the function of ER resulting in stress, which promotes the excretion of the excessive lipids from the liver into circulation without improving hyperinsulinemia [89].

A study has revealed that mice with the absence of C/EBP homologous protein (CHOP$^{-/-}$) in mice has no ectopic fat depositions, no elevated inflammation and maintains normal glucose homeostasis; this study has also demonstrated that the development of insulin resistance is because of ectopic fat deposition that produces pro-inflammation [70], assuming that ectopic fat deposition that produces pro-inflammation is the major factor to induce insulin resistance. CHOP is also responsible for regulating ER stress interceded apoptosis [70].

Eukaryotic cells have a system to alleviate ER stress called the unfolded protein response (UPR). There are three major transducers of UPR: PKR like ER kinase (PERK), inositol requiring enzyme 1 (IRE1), and activating transcription factor 6 (ATF) [90]. ER stress is associated with the induction of massive amounts of pro-inflammatory proteins through the three UPR transducers. One of the pathways is PERK-eIF2α; in this pathway, eIF2α inhibits the IκB protein, which releases the transcription factor NFκB to the nucleus and promotes the expression of pro-inflammatory proteins [88]. PERK-eIF2α-ATF5 and IRE-1 pathways induce TXNIP-NLRP3 protein, which directly causes induction of the pro-inflammatory protein IL-1β; IRE-1 also induces the pathways of IKKβ, XBP1s, and JNK to promote inflammation [88]. ATF6 also induces inflammation, but the mechanism is unknown [91]. The excess

pro-inflammation due to lipid accumulation in the ER leads to the development of insulin resistance in the long run.

2.1.4.5 Lysosomal dysfunction: The lysosome is another important organelle in a eukaryotic cell. Its function is to degrade and recycle long-lived, unnecessary/dysfunctional proteins, lipids and organelles; and generate ATP, new lipids, proteins, organelles, and excretion of cell debris by this process is called autophagy [92, 93]. The process of autophagy is essential in order to attenuate stress, remove ROS, and maintain cellular homeostasis. During excess carbohydrate and amino acid consumption, one of the central regulatory proteins, Mammalian Target of Rapamycin (mTOR), is increased, which inhibits autophagy [94]. On the contrary, during nutrient deprivation, AMP-dependent protein kinase (AMPK) increases through the inhibition of mTOR and activates autophagy [95-97]. Several studies suggest that mTOR is a major autophagy regulator. Elevation of lipid levels increase the release of FFAs from dysfunctional adipocytes, suppressing autophagy by improving the function of autophagolysosome, hydrolase activity, and lysosomal acidifications [98, 99]. Liver-specific knockout *atg7* and *tfeb* genes (associated with autophagy) in diet-induced obese mice promotes liver steatosis, and overexpression of these genes prevent weight gain and metabolic abnormalities [100, 101], indicating that obesity suppresses autophagy in the liver. Another potential mechanism is that obesity hampers de-nitrosylation capacity through inhibiting *S*-nitrosoglutathione reductase (GSNOR) in the liver which controls the access of NO in the liver cells; excess NO induces s-nitrosylation causing nitrosative stress which causes dysfunction in lysosomes and lysosomal autophagy [102]. The defective hepatic autophagy increases the accumulation of misfolded/unfolded proteins and lipids, which promotes ER stress and dysfunction of the mitochondria. This leads to chronic inflammation leading to insulin resistance. The processes are entirely opposites when adipose tissue-specific deletion of the *atg7* gene decreases adipose tissue content

and increases insulin sensitivity [103, 104]; however, the precise mechanism is unknown. The overload of lipids in obese adipose tissues induces lipophagy (an autophagy process to recycle and scavenge unusual and extra lipids); because of lipid congestion, the lipophagy flux may be suppressed which creates complexity, inducing ROS and intense pro-inflammation. Interestingly, most of the studies have demonstrated that obesity upregulates autophagy in the adipose tissue whereas it downregulates autophagy in the liver and pancreas, and there is no effect of obesity-associated autophagy on muscle tissues [92, 105].
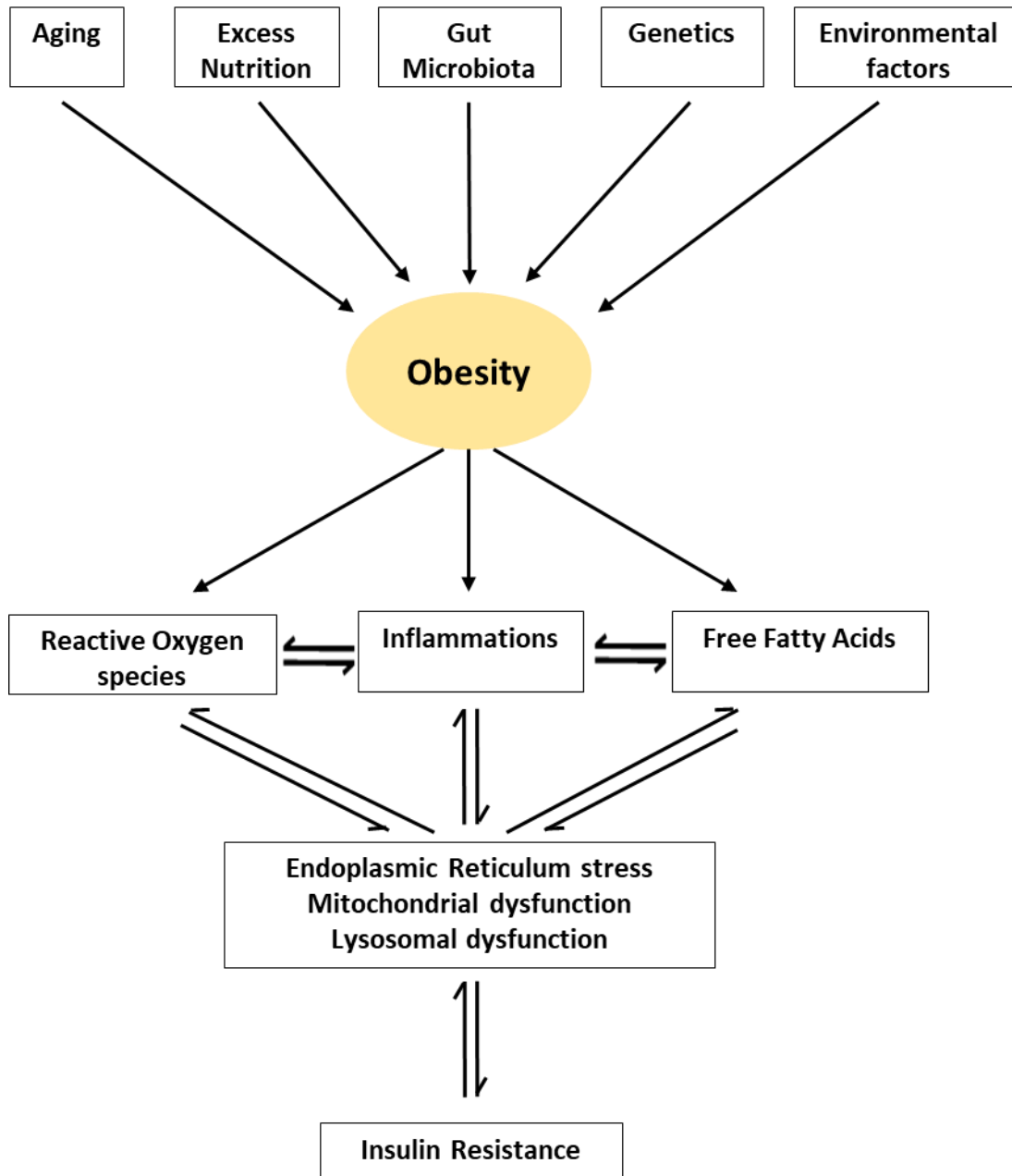
Fig 2.1: Complication of obesity linked insulin resistance

2.2 What is Cancer?

Cancer is the uncontrolled growth of abnormal cells with potential to invade and spread to the other parts of the body. The tumor develops when a cell's normal control mechanism dysfunctions. Normal cells go through aging and apoptosis process, whereas cancer cells form mass tissue by an accumulation of abnormal cells, which is called a tumor. Tumor growth can be divided into two types, one is a malignant and benign [106]. The benign tumor grows very slowly and usually does not make any problems. Usually, they are not life-threating, but if the benign tumor grows more than usual, it can block the function of tissue or become malignant after a certain period. The malignant tumors are life-threating, invade the surrounding tissues, and metastasize to distant locations in the body. When a malignant tumor starts growing, their characteristics have changed far from normal cells. These types of tumors create their own blood vessels so that the tumors can get enough nutrients for their continuous growth and development. The process of blood vessel development is called angiogenesis[106]. At a certain time point, tumor cells do not adhere together, but instate breakaway, spread through the lymphatic system and start growing somewhere else in the body; this process is called metastasis[106]. The malignant tumor is called cancer. There are more than 200 types of cancer; the types are dependent upon location in specific tissues or organs. For example, colorectal cancer starts growing from the cell of the colon and rectum; lung cancer starts growing from cell of the lung. Cancer is also categorized by the types of cells from which they arise. Carcinomas are the common type of cancer formed by epithelial cells. Sarcomas form in bone and soft tissues, including muscle, fat, blood vessels, lymph vessels, and fibrous tissue. Osteosarcoma is the most common soft tissue sarcoma of the bone. Leukemia begins in the blood-forming tissue of the bone marrow, and this type of cancer does not form a solid tumor. Lymphoma is formed in lymphocytes such as T cells or B cells, abnormal lymphocytes build up in lymph nodes, lymph

vessels, and other organs of the body. Melanoma starts forming on the pigment tissues, such as the tissues that make melanin or skin color.

2.2.1 Cancer epidemiology

Recent data has shown that the overall cancer incidence rates for all ages during 2011–2015 was 494 among male patients and 420 among female patients in 2016 per 100,000 [107]. The overall cancer death rates of all ages were 193 among male patients and 137 among female patients (per 100,000) during 2012 [107]. The highest incidences of cancer among men between the ages of 20-49 were colorectal cancer, testis, and melanoma of the skin. The incidences of cancer among women were breast, thyroid, and melanoma of the skin [107]. Based on the data from 2013–2015, it is suggested that approximately 38.4% of men and women will be diagnosed with cancer at some point during their lifetime [107]. More than 15 million Americans have a history of cancer and will experience in their lifetime, which has a tremendous financial impact. In 2014, US, cancer patients paid $4 billion out of pocket for cancer treatment, and roughly $87 billion was spent on the cancer-related health care cost by the insurance companies, employs, and public programs [108].

2.2.2 Driver of cancers

There are three main types of genes are affected during cancer development: proto-oncogenes, tumor suppressor genes, and DNA repair genes. These changes are sometimes called the driver of the cancer [109]. Proto-oncogenes are involved in normal cell growth and development. The mutation of these genes gives rise to oncogenes which are active, which allow the cell to grow, survive, and inhibit apoptosis [110]. Examples of proto-oncogenes are RAS, WNT, MYC, ERK, and TRK. Tumor suppressor genes are involved in controlling cell growth and division. Unlike oncogenes, tumor

suppressor genes generally follow the "two-hit" hypothesis [111]. In this theory, both alleles that code for a particular protein must be mutated or affected before the cause the cell to uncontrollably proliferate. Examples of tumor suppressor genes are TP53 PTEN, pVHL, APC, CD95 ST5, YPEL3, ST7, and ST14. DNA repair genes are involved in fixing the damaged DNA. Sometimes these genes are classified as tumor suppressors as the mutation of these genes decrease DNA repair leading to increased inactivation of other tumor suppressors and pro-oncogenes [112]. Some of the DNA repair genes are HNPCC, MEN1, and BRCA.

2.3 Colorectal cancer

Colorectal cancer develops in the colon and rectum. The colon cancer and rectum cancer are grouped together because of the commonality between them. CRC is the third most common cancer diagnosed and fourth most cancer related to death worldwide, which leads to about 1.4 million new cancer cases and almost 70,000 deaths [9]. The burden of CRC is expected to increase by 60% by 2030, which is about 2.4 million new cancer cases and 1.1 million cancer deaths [113]. Usually, CRC develops from benign pre-cancerous polyps. These types of polyps are localized abnormal cells in the intestinal mucus, which then multiplies and protrudes into the intestinal lumen. With time, the abnormal cells undergo sufficient genetic changes, resulting in larger tumors which acquire the ability to grow on the bowel wall: this is a hallmark of CRC. Eventually, the CRC cells spread to the lymph nodes and other organs such as live [1]. CRC grows very slowly; symptoms do not become apparent until the tumor becomes several centimeters in diameter which may block the movement of feces, leading to pain, bleeding, and cramping. Usually, it takes several years to a decade for a polyp to acquire the CRC features [114].

2.3.1 Stages of colorectal cancer

Staging is a process use to describe how much cancer is in the body, how serious the cancer is, and how best it is to treat. The earliest stage of colorectal cancer is called stage 0 and then ranges from stages I through IV [115]. The staging of CRC is as follows (Fig 2.2).

Stage 0: initially, abnormal cells develop in the mucosa (which is the innermost layer of the colon/rectum wall). This state is also called carcinoma in situ.

Stage I: cancer develops in the mucosa and spreads to the submucosa (which is a layer of the tissue near to mucosa) or muscle layer.

Stage II is divided into three stages: IIA, IIB, and IIC. In Stage IIA, Cancer spreads through the muscle layer to the serosa (which is the outermost layer). In stage IIB, cancer spreads through the serosa to nearby tissues, but has not spread to adjacent tissue. In stage IIC: cancer spreads through the serosa to nearby organs.

Stage III is divided into three stages: IIIA, IIIB, and IIIC. In stage IIIA, Cancer spreads from the mucosa to the submucosa, the muscle layer, or 1 to 3 nearby lymph nodes. In stage IIIB, Cancer spreads from the muscle layer to the serosa, the serosa to the tissue that lines the organs in the abdomen (which is the visceral peritoneum), 1 to 3 nearby lymph nodes, nearby tissues, 4 to 6 nearby lymph nodes, or 7 to more nearby lymph nodes. In stage IIIC, cancer spreads through the serosa to the visceral peritoneum, 4 to 6 nearby lymph nodes, through the muscle layer to the serosa, serosa to the visceral peritoneum, 7 to more

nearby lymph nodes, through the serosa to nearby organs, or develop cancer cell near the lymph node tissue.

Stage IV is divided into three stages: IVA, IVB, and IVC. In the stage IVA: cancer spreads at least one distance area, or organ, such as the lung and liver. In the stage IVB: cancer spreads more than one distance area, or organ. In stage IVC: Cancer spreads to the distant parts of the peritoneum, or may have spread to other areas, or organs.
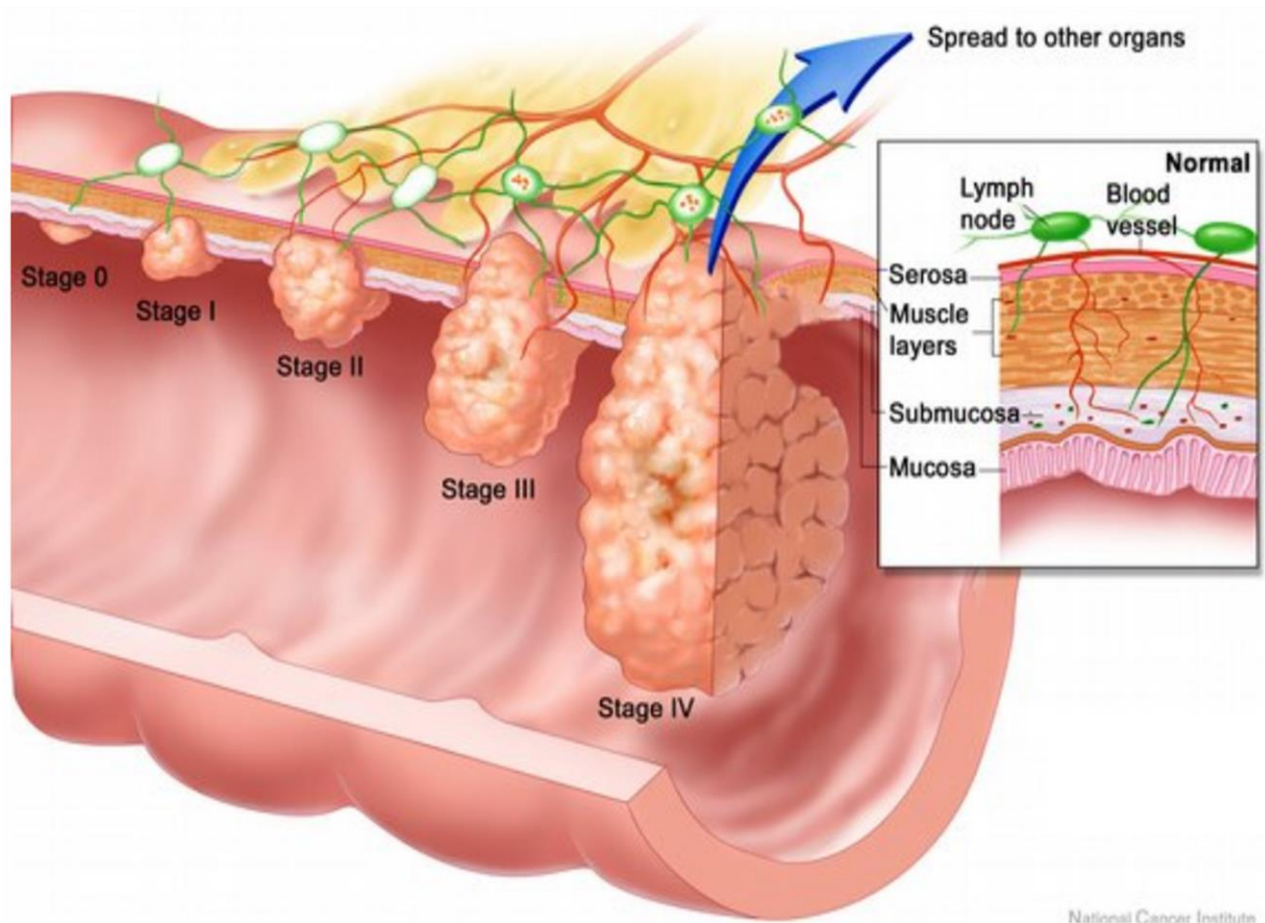
Fig 2.2: Stages of colorectal cancer [1]: In stage 0, abnormal cells form in the the mucosa / innermost layer. Stage I: cancer has grown through the mucosa to the muscular layer. Stage II: cancer has spread through the muscle layer to the outmost layer of colon or rectum. Stage III: The tumor has spread through the wall to at least 1 to 3 lymph nodes and/or the surrounding organs, but it has not spread to the distant organ. Stage IV: cancer has spread to other parts of the body.

2.3.2 Molecular subtyping of colorectal cancer

Molecular subtyping of CRC was performed to characterize the key biological features of CRC in core subtypes, and assess whether the subtype assignment correlated with patient outcome. Gene expression-based cancer subtyping is widely accepted, because different data processing and algorithm techniques are used for subtyping diverse sets of data from different cohort and genome studies; it is challenging to use the data in translational and clinical utility. Guinney et al. [116] analyzed data from independent molecular classification systems, and they developed classification from six different gene expression data sets and unified a single consensus system that had four distinct groups (Fig 2.3). Four consensus molecular subtypes (CMSs) are: CMS1, CMS2, CMS3, and CMS4.

Approximately 14% of all CRC are considered in the CMS1 subtype, of which 12% are sporadic and remain inherited. The characteristics of CMS1 subtypes are being located in the proximal colon, having a high BRAF mutation rate, associated with impaired DNA mismatch repair (MMR), and has a CpG island hyper-methylation.

Approximately 39% are considered in the CMS2 (canonical) subtype. The CMS2 subtype of cancer arises from the canonical adenoma to carcinoma pathway. The characteristic of this CMS2 subtypes are the initial loss of APC as a tumor suppressor gene, followed by mutating KRAS and loss of TP53.

Approximately 13% of all CRC are considered in the CMS3 subtype. The have chromosomal instability (MSI) but low copy number alterations (SCNA) than CMS1 and CMS2. The characteristics of CMS3 are that of 30% CMS3 are hyper-mutated and of 68% CMS3 has *KRAS* mutation.

Approximately 23% of all CRC are considered in the CMS3 subtype, and typically has a high TGFβ concentration in precancerous condition. Characteristics of CMS4 are microsatellite stable, chromosomal instability, very low levels of hypermutation, and very high levels of SCNA. Genes that are frequently mutated in this CRC subtype include *TP53, KRAS APC*, and *PIK3CA*.

CMS1 MSI immune	CMS2 Canonical	CMS3 Metabolic	CMS4 Mesenchymal
14%	37%	13%	23%
MSI, CIMP high, hypermutation	SCNA high	Mixed MSI status, SCNA low, CIMP low	SCNA high
BRAF mutations		*KRAS* mutations	
Immune infiltration and activation	WNT and MYC activation	Metabolic deregulation	Stromal infiltration, TGF-β activation, angiogenesis
Worse survival after relapse			Worse relapse-free and overall survival

Fig 2.3: Molecular subtypes of CRC

2.3.3 Obesity-associated cancer

The prevalence of obesity is continuously increasing, which is alarming; about 39.8% of adults are considered to be obese in the US [2]. Obesity is recognized to be a serious public health problem that is becoming more prevalent worldwide. It is associated with increased risk of a number of medical problems such as: type II diabetes, cardiovascular diseases, and cancer. According to CDC news, 40% of overweight and obese individuals develop cancer in the US [117]. Excess body weight is the most prevalent risk of cancer in high-income countries [118]. The global epidemiological and cancer transition studies suggest that the epidemic is also extending to the developing world [119]. A systematic review concluded that increased 5 kg/m^2 BMI had the strongest effects on risk of developing several types of cancer in men, including esophageal adenocarcinoma, thyroid cancer, and colon cancer[8]. A large prospective study of the Swedish Obese Subjects was convinced that bariatric surgery reduced 20 kg weight in women with the BMI higher than 40 kg/m^2; the surgery reportedly reduced cancer frequency in association with considerable weight loss in a follow-up post-surgery longer than ten years [120].

2.3.4 Obesity-associated colorectal cancer:

Recent epidemiological and experimental evidence indicates that obesity and its metabolic abnormalities are associated with CRC [121]. CRC is also a major public health concern and one of the leading causes of cancer death. The incidence rate of both CRC and obesity is high in developed countries, and obesity has been consistently an identified risk factor for CRC. CRC is one of the most prevalent diseases associated with cancer [122]. Obesity is significantly associated with a 30%-70% [123] increase in CRC risk compared to normal weight, but the pathophysiology remains undefined. In the case of teenagers, excess body weight increases the mortality rate, which is doubled in adulthood [124]. Moreover, a

clinical study found that diet-induced weight loss reduced CRC related colorectal inflammation and gene expression [125].

Obesity is accompanied by some degree of inflammation called chronic low-grade inflammation, which is considered to be a protective mechanism. With excess weight gain, adipocytes increase in size, leading to an inadequate supply of oxygen (hypoxia) as well as infiltration of macrophages into the adipose tissues, which is accompanied by an elevated adipocyte cell death. Obese adipocytes release adipokines (MCP-1, TNF-α, IL-6, and IL-1β) and free fatty acids (FFA) which interact with TLR4 complex in resident macrophages, which activates the transcription factor NFkB. Activated NFkB promotes pro-inflammatory proteins both in the adipocytes and resident macrophages in adipose tissue. Activated macrophages in the adipose tissue aggravate the release of pro-inflammatory cytokines such as MCP-1, TNF-α, IL-6, and IL-1β, which results in the polarization of anti-inflammatory M2 macrophages to pro-inflammatory M1 macrophages [126]. While adipose tissue macrophages (ATM) represent less than 10% of all adipose tissue cells in lean mice and humans, their percentage may raise over 50% in extremely obese mice and nearly 40% in obese humans [127]. It has been reported that macrophages treated with glucose, insulin, and fatty acids (palmitate) can drive the pro-inflammatory ATM phenotype in obese mice [128]. Excess lipid accumulation and induction of inflammation by macrophages may result in impaired insulin signaling through cell-autonomous mechanisms.

Many of the cytokines and growth factors synthesized and released by adipose tissues have direct pro-tumorigenic effects in the gastrointestinal tract [14]. The number of macrophages with the M1 phenotype increases rapidly during chronic inflammation, and it may result in predestination of a given tissue to tumor initiation by the release of factors that promote neoplastic transformation[123]. The tumor-

associated macrophages (TAMs) express the M2 phenotype, promote tumor cell survival, and contribute to tumor growth, vascularization, and progression [129, 130]. Macrophages have been shown to infiltrate a CRC tumor [131]. A high density of TAMs has been significantly associated with poor prognosis in a majority of tumors; however, the invasiveness of CRC cells and their ability to metastasize to other organs is associated with the ratio of M2 to M1, but not the number of M2 phenotype cells [132]. Macrophage polarization in adipose tissue is similar to that in cancer, where the polarization of macrophages toward the pro-inflammatory phenotype has been established [133]. It has been shown that high-fat diet-fed mice develop an insulin resistant and pro-inflammatory environment, which can promote CRC tumor growth compared to control diet mice [15].

It is also demonstrated that obesity-induced IL-6 as a modulator of the tumor microenvironment in colitis-associated CRC by macrophage polarization and successive lymphocyte recruitment [134]. The secretion of IL-1β from tumor cells into the tumor environment also promotes several angiogenic factors, not only from tumor cells but also from stromal cells, including fibroblasts and macrophages, and in this way stimulates tumor neovascularization[135].

Obesity not only provides a microenvironment that make tumor cells make aggressive [136-138] but also adipocyte cells absorb two commonly used chemotherapy drugs and break them down chemically into less toxic forms, potentially reducing the drug's effectiveness [139]. CRC is one of the costliest types of cancers; the second is breast cancer which poses a significant economic challenge to the health care industry. The national public burden of disease remains seriously high for CRC with both the direct and indirect costs associated with CRC screening, and treatment is estimated to be upwards of $17 billion by 2020 [10]. The future development for treatment is becoming more target-specific in CRC. Thus, the

mechanism behind obesity-associated CRC and the identification of novel therapeutic targets for CRC is critical for future therapeutic treatments.

Chapter 3: TNF-α and hypoxia induced long-term insulin resistance in differentiated 3T3-L1 adipocytes *in vitro*.

3.1 Abstract

Recently, obesity has become an epidemic. In the obese condition, cells become resistant to insulin. The adipose tissues play a leading role in developing obesity-linked insulin resistance. Epidemiological studies have demonstrated that the obese insulin resistant environment is associated with the development of numerous clinical conditions. In this study, we aimed to investigate the ability of TNF-α and hypoxia to induce insulin resistance in 3T3-L1 differentiated adipocytes, and to develop a long-term insulin resistant model in the 3T3-L1 differentiated adipocytes. 3T3-L1 cells (pre-adipocytes) were differentiated to become mature adipocytes. Cells were treated with low glucose serum-free media containing 20ng/ml TNF-α and kept in a hypoxic chamber with 1% O_2 & 5% CO_2 for 24 hours to induce insulin resistance. After 24 hours, 4.5g/L glucose and 10% FBS were added to the treated adipocytes to obtain viable cells in the insulin resistance state throughout 72 hrs. RT-qPCR, western blot, and Oil red O were performed to assess the phenotype of treated the adipocytes. Results showed that TNF-α and hypoxia significantly reduced the expression of insulin sensitive genes *adipoq* and *slc2a4* in differentiated adipocytes for three days. On the other hand, TNF-α and hypoxia significantly induced the expression of the insulin resistance genes *ccl2* and *IL6* for three days consistently. Oil red O staining results showed that differentiated adipocytes lost lipid content overtime because of insulin resistance. To confirm the insulin resistance phenotype, we conducted an in vitro insulin sensitivity test. In this test, serum-deprived treated cells were induced with 50 nM insulin for 15 min; insulin signaling markers were assessed by western blot. We found that phosphorylation of AKT in treated adipocytes was significantly decreased compared to untreated adipocytes. We concluded that the combination of TNF-α and hypoxia

have the capacity to induce long-term insulin resistance *in vitro*, and our long-term insulin resistance

model may serve as a platform to examine the mechanism of obesity-associated diseases.

3.2 Introduction

Obesity causes a severe public health problem and has become an epidemic worldwide. The rate of obesity is increasing alarmingly; data shows that 39% of adults are considered to be obese in the US [31]. Obesity plays a pivotal role in the development of insulin resistance, which is the risk factor for many chronic diseases such as cancer, type 2 diabetes, hypertension, atherosclerosis, and cardiovascular diseases [5]. Insulin resistance develops when insulin-sensitive tissues loss their response to insulin.

3T3-L1 is a cell line developed from mouse 3T3 cells. These cells have the morphology of fibroblast cells, but under a specific condition; these cells can differentiate into adipocytes by synthesizing and accumulating triglycerides [140]. Differentiated 3T3-L1 adipocytes are highly insulin sensitive and as such have the ability to develop an insulin resistant phenotype. Studies have shown that many molecules have the capacity to induce insulin resistance in differentiated 3T3-L1 adipocytes such as IL6, IL-1, TNF-α, FFAs, dexamethasone, high insulin, glucosamine, growth hormone, and hypoxia [141]. A recent study demonstrated that the combination of TNF-α and hypoxia were able to induce insulin resistant in differentiated 3T3-L1 adipocytes *in vitro* that mimicked the adipose tissue of *in vivo* diet-induced obese insulin resistance mice [141]. TNF-α is one of the first molecules that was shown to induce insulin resistance: it's mode of action is to suppress fatty acid uptake and promote lipolysis in adipose tissue [142]. Hypoxia is also one of the key regulatory factors in obesity that promotes adipose tissue dysfunction by dysregulating insulin signaling through the transcription factor *HIF* and as such induces insulin resistance [143].

To demonstrate the pathophysiology of obese insulin resistance states associated clinical conditions, and to screen the therapeutic agents, it is essential to have an *in vitro* insulin resistance model so that the

model can serve as a platform. The advantage of the in vitro model is, the technique is performed in a controlled environment outside of a living organism. There is a lacking of an long-term obese insulin resistance model *in vitro* for the therapeutic and mechanical approach. Therefore, firstly, our aim is to confirm the capacity of TNF-α and hypoxia to induce insulin resistance in the differentiated 3T3-L1 adipocytes *in vitro.* Secondly, our aim is to investigate the capacity of TNF-α and hypoxia to establish a long-term obese insulin resistance model *in vitro*. If successful, our platform has the capacity to examine the mechanism of obesity-associated pathophysiology. Our data demonstrates that it is possible to develop a long-term obese insulin resistance model *in* vitro.

3.3 Materials and Methods

3.3.1 Reagents

3T3-L1 preadipocytes were purchased from the American Type Culture Collection (ATCC, Manassas, VA, USA). Dulbecco's modified Eagle's medium (DMEM), glutamine, and penicillin-streptomycin (P/S) were obtained from Gibco (Grand Island, NY, US). Trypsin/EDTA and fetal bovine serum (FBS) were obtained from LONZA (Walkersville, MD, US) and ATLANTA Biologicals (Lawrenceville, GA, US), respectively. Insulin was from Roche (Mannheim, Germany). 3-isobutyl-1-methylxanthine (IBMX), dexamethasone, and rosiglitazone were from Sigma (St Louis, MO, US). Pierce BCA protein assay kit was purchased from ThermoFisher Scientific (Rockford, IL, US). Primary antibodies protein kinase B (AKT) and phosphyorylated AKT were purchased from Cell Signaling Technology (Beverly, MA, US). Secondary antibody goat anti-mouse IgG IRDye 680RD and goat anti-rabbit IgG IRDye 680RD were obtained from LI-COR (Lincoln, NE, US). TRIzol reagent was purchased from Invitrogen (Carlsbad, CA, US). Reverse transcription RT2 HT First Strand and SYBR Green qPCR Mastermix kits were purchased from Qiagen (Valencia, CA, US), respectively. Mouse primers *b-actin*, *GAPDH*,

Adipoq, IL6, and *ccl2* were purchased from Sigma (St Louis, MO, US). Oil Red O solution was from Electron Microscopy Sciences (Hatfield, PA, US). Phosphate-buffered saline (PBS) and 2-propanol were from Fisher Scientific (Pittsburgh, PA, US).

3.3.2 3T3-L1 cell culture

3T3-L1 cells (pre-adipocytes) were cultured in high glucose DMEM media containing 4.5g/L glucose, 10% FBS, and 1% P/S in 6-well plates. Pre-adipocytes were seeded in 6 well plates and allowed to grow until the cells were reached to 100% confluence, then a cocktail of 0.5mM IBMX, 1μM dexamethasone, 1μM rosiglitazone and 10μg/mL insulin was used for three days to induce adipocyte differentiation which we designated as "Day 0" of differentiation. On day three post differentiation, fresh media containing high glucose was replaced every two days until day ten. Cells were treated with low glucose serum-free media containing 20ng/ml TNF-α and kept in a hypoxic chamber with 1% O_2 & 5% CO_2 for 24 hours to induce insulin resistance [141]. 4.5g/L glucose and 10% FBS were then added to the treated adipocytes to obtain viable cells in the insulin resistance state over the course of 72 hrs. Untreated differentiated adipocyte served as control insulin sensitive cells.

3.3.3 Oil Red O staining

Differentiated adipocyte samples were washed with 1X PBS two times. Cells were fixed with 10% formalin in PBS for one hour at 4°C and then washed twice using distilled water. The cells were stained with 60% Oil Red O solution (0.5mL/well) for 15 min at room temperature and then washed thrice with distilled water. Images were obtained using a Nikon Ti Eclipse at day 10, treated adipocytes at day 3 and untreated adipocytes at day 3.

3.3.4 Western blot

Differentiated adipocytes were collected in RIPA buffer directly, and sonication was performed for 30 sec in 5-sec intervals (5-sec sonication and 5 sec on ice for three times). Protein concentration was measured by the Pierce BCA protein assay kit. Prior to gel electrophoresis, an equal amount of protein sample was heated at 70°C for 10 min in sample buffer [144]. Protein in the samples was separated using 10% polyacrylamide gel electrophoresis at 100mA for two hours and then transferred to nitrocellulose membranes at 100mA for two hours at 4°C. The membrane was blocked with tris-buffered saline with 0.1% Tween20 (TBST) containing 5% skim milk at room temperature for one hour. Following this, the membrane was incubated overnight with the relevant primary antibody at 4°C and then incubated with a secondary antibody for one hour at room temperature. The membrane was analyzed in a Li-COR blot scanner. Band intensities were quantified by the Imagestudio software (LI-COR Biosciences, NE, US).

3.3.5 Quantitative polymerase chain reaction

Total RNA was extracted from differentiated adipocytes using TRIzol reagent. RNA was reversed transcribed using an RT2 HT First Strand kit. Quantitative polymerase chain reaction (qPCR) amplifications were performed using qPCR Mastermix. The following amplification conditions were used with 40 cycles of 15 seconds of denaturation at 95°C, followed by 1-minute annealing. Primers are shown in Table 3.1. Reactions were performed in triplicate, and data were calculated by the ΔΔCt method. Eef2 (Eukaryotic Translation Elongation Factor 2) and GAPDH (Glyceraldehyde 3-phosphate dehydrogenase) reference genes normalized gene expression.

Table 3.1 Quantitative PCR primers		
Genes		**Sequence (5′-3′)**
Ccl2 (MCP1)	Forward	caagatgatcccaatgagtag
	Reverse	ttggtgacaaaaactacagc
Slc2a4 (GLUT4)	Forward	caatggttgggaaggaaaag
	Reverse	aatgagtatctcataggaggc
Adipoq (Adiponectin)	Forward	ccactttctcctcatttctg
	Reverse	ctagctcttcagttgtagtaac
IL6	Forward	aagaaatgatggatgctacc
	Reverse	gagtttctgtatctctctgaag
Eef2	Forward	agaacatatattgctggcg
	Reverse	caacagggttagatttcttg
GAPDH	Forward	
	Reverse	

3.3.6 Statistical analysis

All experiments were run at least in triplicate. After checking for normal distribution, data were analyzed using either t-test or one way ANOVA with Tukey post-hoc test depended upon the group of samples**.** P-values less than 0.05 was determined to be a significant.

3.4 Results

3.4.1 TNF-α and hypoxia successfully induced insulin resistance *in vitro*

3.4.1.1 TNF-α and hypoxia reduced insulin-sensitive gene expression: To develop an insulin resistant model *in vitro*, differentiated adipocytes were treated with a different combination of TNF-α and hypoxia. We found that individual 20ng/ml TNF-α treatment significantly (p=0.001 and p=0.001, respectively) decreased the expression of insulin-sensitive genes *adipoq* and *slc2a4* by the fold change 0.13±0.0 and 0.27±0.1, respectively (Fig 3.1). In the case of hypoxia, the expression of insulin-sensitive genes *adipoq* and *slc2a4* (p=0.001 and p=0.001, respectively) significantly decreased by the fold change 0.01±0.0 and 0.01±0.0 respectively. When the adipocytes were treated with combined TNF-α and hypoxia the expression of *adipoq* and *slc2a4* were significantly (p=0.001 and p=0.001 respectively) decreased by the fold change 0.00±0.0 and 0.01±0.0 respectively, which was the lower than others individual treatments.

3.4.1.2 TNF-α and hypoxia-induced insulin resistance gene expression: We also assessed pro-inflammatory markers associated with insulin resistance; we did not find any significant difference in *ccl2* and *IL6* expression when differentiated adipocytes were treated with individual TNF-α and hypoxia. However, the combined TNF-α and hypoxia significantly (p=0.001 and p=0.001 respectively) increased *ccl2* and *IL6* by the fold change of 14.98±1.25 and 8.82±0.47, respectively (Fig 3.2).

3.4.1.3 TNF-α and hypoxia successfully induced insulin resistance *in vitro*: To further assess the insulin resistance phenotype of the adipocytes, after 24 hours of treatment with combined TNF-α and hypoxia, cells were induced by 50 nM insulin for 15 min. AKT activation was assessed by western blot using an antibody that recognizes Ser 473 phosphorylation [145]. We found that phosphorylated AKT expression significantly (p=0.001) decreased in adipocytes treated with TNF-α and hypoxia compared to untreated adipocytes (Fig 3.3). From this experiment, we demonstrate that TNF-α and hypoxia inhibit insulin signaling.
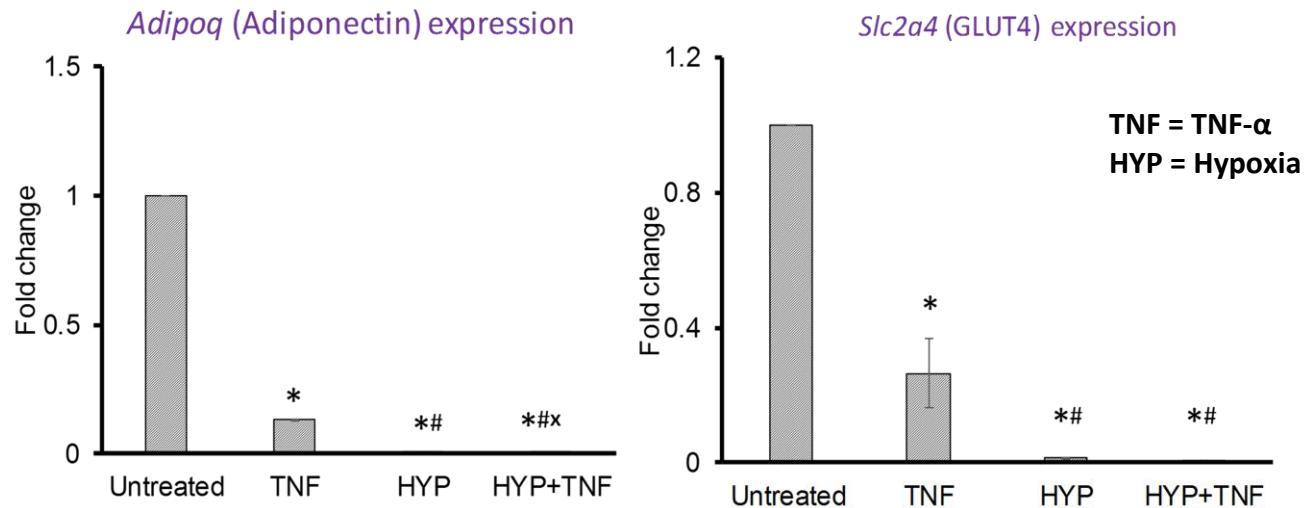
Fig 3.1: TNF-α and hypoxia reduced *adipoq* and *Slc2a4*: Mature differentiated 3T3-L1 adipocytes were treated with TNF-α and/or hypoxia for 24 hours. Insulin sensitive gene markers *adipoq* and *Slc2a4* were assessed using **RT-qPCR.** Gene expression was normalized using *eef2* and *GAPDH* as reference genes, and the ΔΔCt method was used to assess fold changes. Data were analyzed using one-way ANOVA with Tukey post-hoc test. *p<0.05 significant difference compare to untreated group, #p<0.05 significant difference compare to TNF group, xp<0.05 significant difference compare to HYP group.
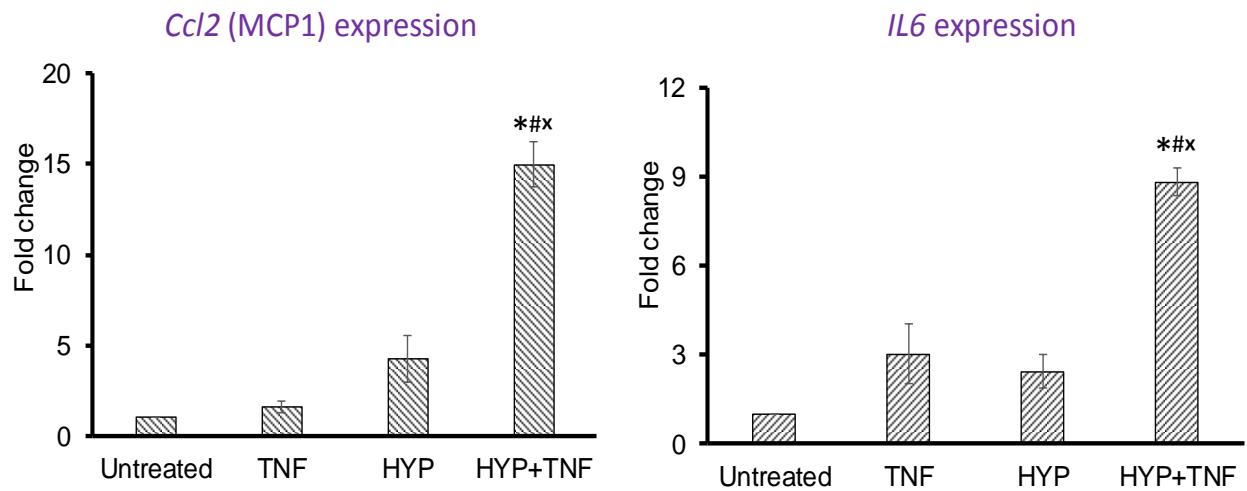
Fig 3.2: TNF-α and hypoxia-induced *Ccl2* and *IL6*: Mature differentiated 3T3-L1 adipocytes were treated with TNF-α and/or hypoxia for 24 hours. Insulin sensitive gene markers *IL6* and *Ccl2* were assessed using **RT-qPCR.** Gene expression was normalized using *eef2* and *GAPDH* as reference genes, and the ΔΔCt method was used to assess fold changes. **Data were analyzed using one-way ANOVA with Tukey post-hoc test. *p<0.05 significant difference compare to untreated group, #p<0.05 significant difference compare to TNF group, ×p<0.05 significant difference compare to HYP group.**
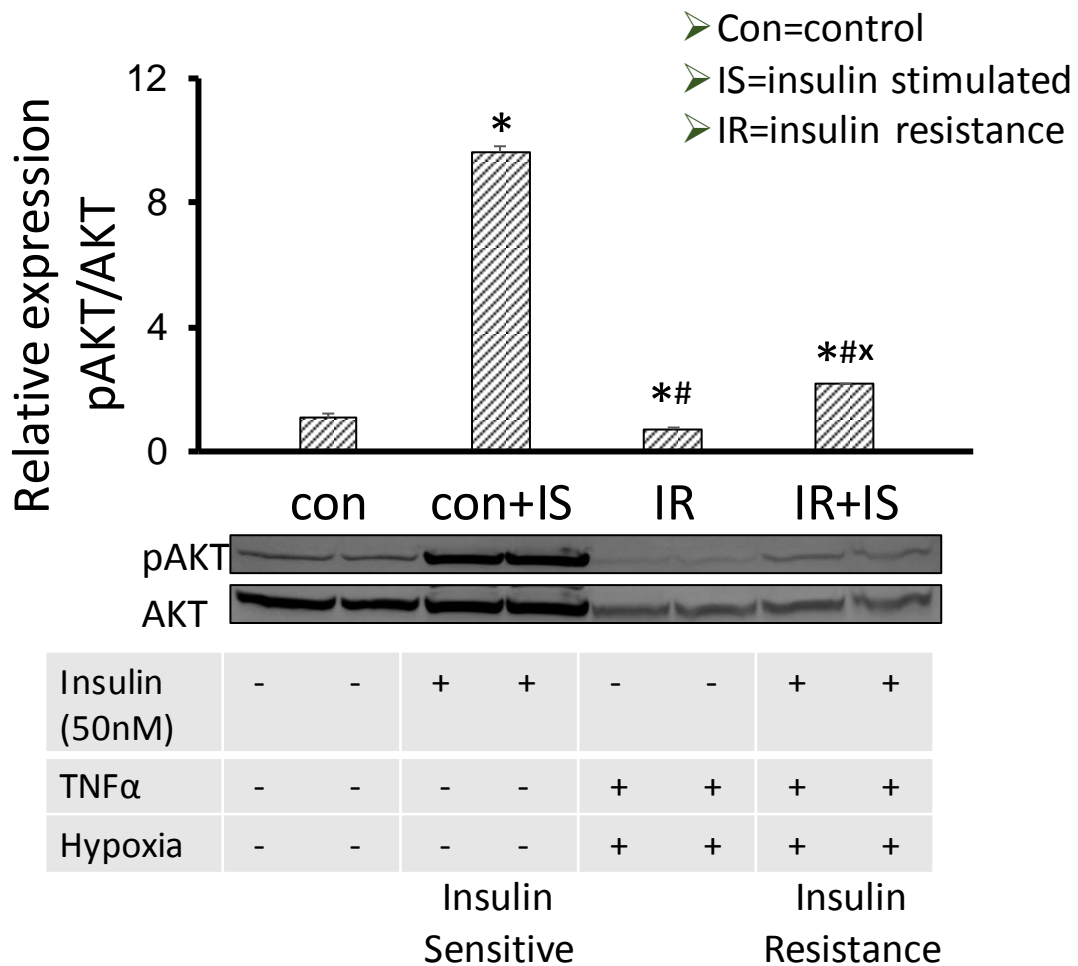
Fig 3.3: Examine insulin sensitivity of the TNF-α and hypoxia treated adipocytes: Mature differentiated 3T3-L1 adipocytes were treated with TNF-α and/or hypoxia for 24 hours. Treated adipocytes were stimulated by 50nM insulin for 15 min. AKT and pAKT markers were assessed using western blot. **Data were analyzed using one-way ANOVA with Tukey post-hoc test. *p<0.05 significant difference compare to con group, #p<0.05 significant difference compare to con+IS group, xp<0.05 significant difference compare to IR group.**

3.4.2 Differentiated adipocytes maintained long-term insulin resistance *in vitro*

Our approach is to develop a long-term insulin resistance model so that the model can be used to serve as a platform to co-culture with 3D engineered CRC patient-derived xenograft (PDX) tissues to examine the molecular mechanism behind obesity-associated CRC.

3.4.2.1 Differentiated adipocytes developed long-term insulin resistance *in vitro:* Differentiated adipocytes were treated TNF-α and hypoxia 24 hours to induce insulin resistance. Extra 4.5g/L glucose and 10% FBS were added to the treated adipocytes after 24 hours to obtain cells in the insulin resistance state through 72 hrs. Samples were collected every 24 hours. We found that both the insulin-sensitive genes a*idpoq* and *slc2a4* significantly (p=0.001 and p=0.001 respectively) decreased by the fold change 0.01±0.0 and 0.14±0.12 at day 1 and the expression was significantly (p=0.001 and p=0.001 respectively) consistent until day 3 by the fold change 0.08±0.06 and 0.19±0.03, respectively (Fig 3.4). On the other hand, the pro-inflammatory gene associated with insulin resistance significantly (p=0.43) increased on day 1 by the fold change 12.85±0.44, and the expression was significantly (p=0.039) consistent at day 3 by the fold change 13.06±1.50.

3.4.2.2 Differentiated adipocytes lost lipid content overtime: To visualize the lipid drop in the treated and untreated adipocytes, we performed Oil Red O staining of the differentiated adipocytes at day ten, at day three of treated adipocytes (TNF-α and hypoxia), and at the day three of untreated adipocytes (which is equivalent to the same age of treated adipocytes). Results showed that the TNF-α and hypoxia treated differentiated adipocytes lose lipid content and appeared to be smaller in size compare to

untreated adipocytes (Fig 3.5). From this experiment, it was concluded that treated cells became insulin resistant because they showed the characteristics of insulin resistance.

3.4.2.3 Differentiated adipocytes successfully developed insulin resistance at day three: To further confirm the insulin resistance microenvironment of the adipocytes, after 72 hours of treatment with combined TNF-α and hypoxia cells were induced by 50nM insulin for 15 min. AKT activation was assessed by western blot using an antibody that recognizes Ser 473 phosphorylation. We found that phosphorylated AKT expression of treated adipocytes (p=0.04) significantly decreased compared to untreated adipocytes (Fig 3.6). From this experiment, it was concluded that TNF-α and hypoxia were able to develop insulin resistance *in vitro* for three days.

Adipoq (Adiponectin) expression

Slc2a4 (GLUT4) expression

Ccl2 (MCP1) expression

T = TNF-α
H = Hypoxia
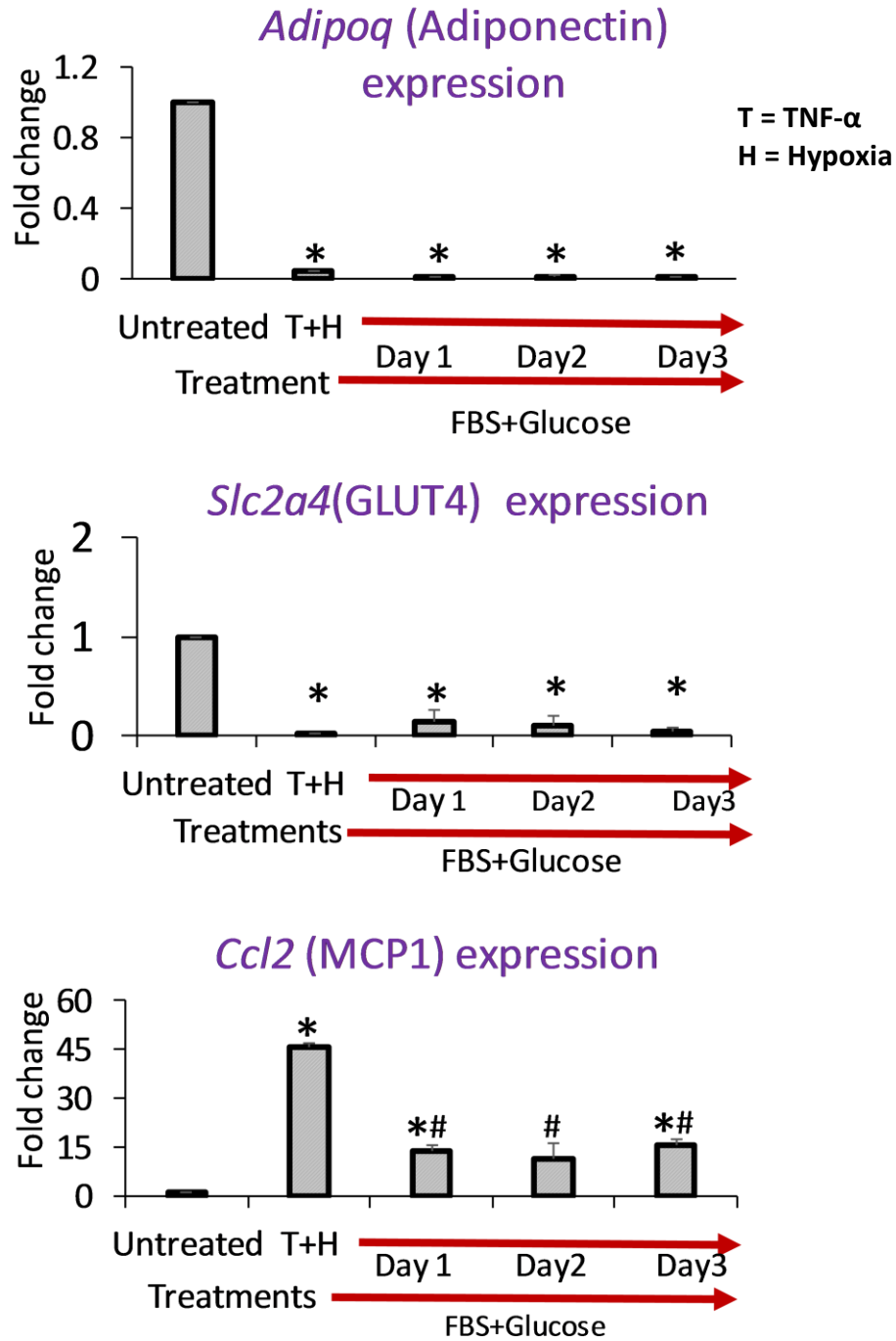
ig 3.4: Demonstration of long-term insulin resistance obese adipocytes *in vitro*: Mature differentiated 3T3-L1 adipocytes were treated with TNF-α and hypoxia for 24 hours. Extra glucose and FBS were added after 24 hours to the IR adipocytes and kept continued another 72 hours. Insulin resistance and sensitive markers *Ccl2, Adipoq*, and *Slc2a4* were assessed using RT-qPCR**.** Gene expression was normalized using *eef2* and *GAPDH* as reference genes, and the ΔΔCt method was used to assess fold changes. **Data were analyzed using one-way ANOVA with Tukey post-hoc test. *p<0.05 significant difference compare to untreated group, #p<0.05 significant difference compare to T+H group.**
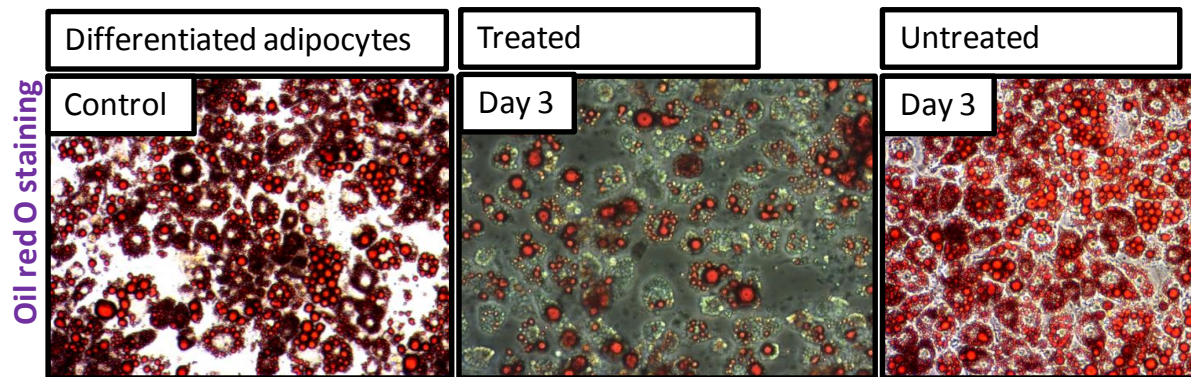
Fig 3.5: Adipocytes lose lipid content overtime because of insulin resistance

microenvironment: Mature differentiated 3T3-L1 adipocytes were treated with TNF-α and hypoxia for 24 hours. Extra glucose and FBS were added after 24 hours to the IR adipocytes and kept continued another 72 hours. Cells were fixed with 10% formalin for 1 hour at 4°C and stained with 60% Oil Red O solution (0.5mL/well) for 15 min. Pictures were taken under a microscope.
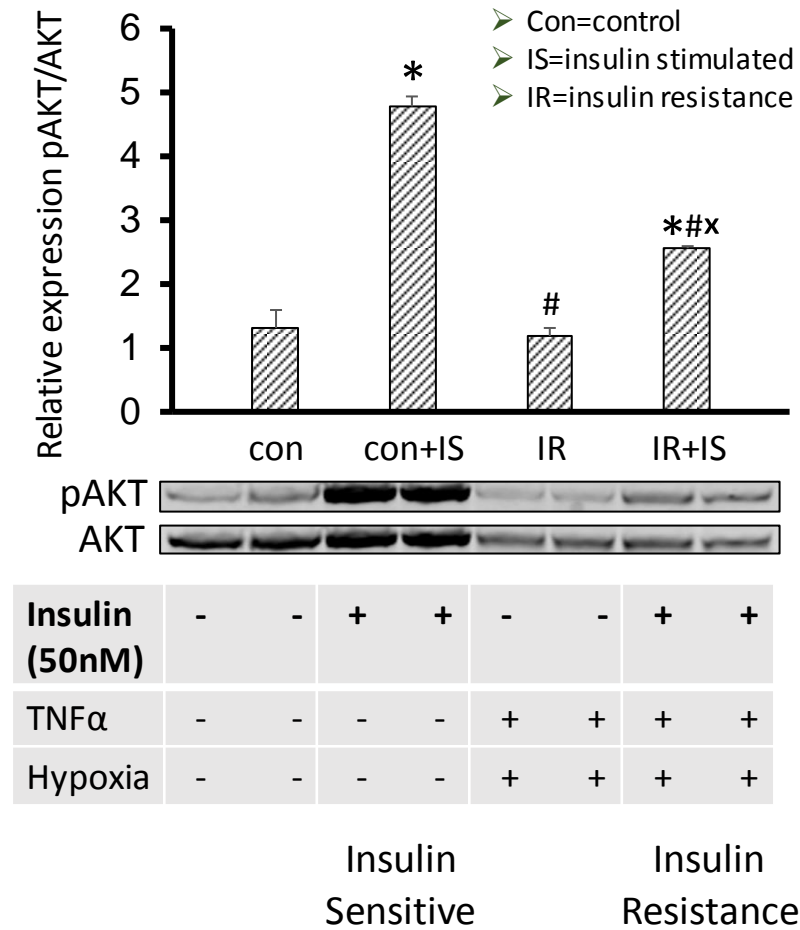
Fig 3.6: Examine insulin sensitivity of adipocyte three days after TNF-α and hypoxia treatment: Mature differentiated 3T3-L1 adipocytes were treated with TNF-α and hypoxia for 24 hours. Extra glucose and FBS were added after 24 hours to the IR adipocytes and kept continued another 72 hours. Treated adipocytes were stimulated by 50nM insulin for 15 min. AKT and pAKT markets were assessed using western blot. Band intensity was measured by the Imagestudio software. Data were analyzed using one way ANOVA with Tukey post-hoc test. *$p<0.05$ significant difference compare to con group, #$p<0.05$ significant difference compare to con+IS group, x$p<0.05$ significant difference compare to IR group.

3.5 Discussion

Obesity is a huge concern worldwide because most obese patients develop insulin resistance at some point. Insulin resistance is associated with several clinical conditions, including type 2 diabetes and cancer, but the mechanism is unknown. The general use of an *in vivo* diet-induced obese insulin resistant mice model has thousands of complex signal processes run at a time that may hinder to demonstrate the direct effect of obese insulin resistance associated diseases. *In vivo* mice studies are also time-consuming and costly. An insulin resistance adipocyte model *in vitro* may facilitate to demonstrate the pathophysiology behind obesity-associated clinical conditions, and also it may expedite the innovation of drugs for novel therapeutic approaches.

In this study, TNF-α and hypoxia were used to develop a long-term insulin resistance microenvironment in the differentiated 3T3-L1 adipocytes. This study demonstrated that TNF-α and hypoxia significantly induced an insulin resistance microenvironment in differentiated adipocytes *in vitro for 24 hours,* and treated adipocytes remained insulin resistance microenvironments for another 72 hours after adding extra FBS and glucose. The results concluded that combined TNF-α and hypoxia have the potency to induce insulin resistance micro-environment *in vitro* in a long-term differentiated adipocytes culture.

In the insulin signaling pathway, insulin activates the insulin receptor causes auto-phosphorylation that changes the conformation of the receptor leading to phosphorylate IRS protein. Phosphorylated IRS protein induces AKT to become phosphorylate AKT. Phosphorylated AKT modulates most of the insulin metabolic effects regulating glucose transport, lipid synthesis, gluconeogenesis, and glycogen synthesis [146]. We observed that a reduction in insulin stimulated AKT phosphorylation was associated with reduced *Slc2a4* gene expression. Transcription factor NFkB is the master regulator of pro-

inflammations; in the diet-induced obese mice, the transcription factor NFkB increases which enhance the production of the pro-inflammatory chemokines and cytokines such as MCP1 (*CCL-2*), IL-6, IL-1β and TNF-α in adipose tissue which promote insulin resistance [147-149]. Our data showed that the treatment of TNF-α and hypoxia significantly induced genes *CCL-2* and *IL-6,* assuming that differentiated adipocytes successfully developed an insulin resistant microenvironment. Adiponectin is a protein hormone that modulates glucose regulation and fatty acid oxidation [150]. Adiponectin increases energy expenditure and reduces adipocytes differentiation; the effect of adiponectin was found to decrease in obese adipose tissue [151], which is also showed in our data.

Multiple studies have been done on the effect of hypoxic conditions on adipocytes and adipose tissues [141, 143, 152-154]. A study has showed that adipocytes exposed to hypoxia for 24 hours *in vitro* have an intense effect on adipocyte dysfunction, which modified at least 1346 genes [153]. Hypoxia treatment in the differentiated 3T3-L1 adipocytes has a rapid and robust impact on the inhibition of insulin signaling through insulin receptor IRS phosphorylation. TNF-α is also widely used to develop insulin resistance [155-157]. Besides inducing insulin resistance on adipose tissues, TNF-α is able to upregulate genes related to chemotaxes such as *ccl2, Ccl7,* and *ccl9* [141]. Chemotaxis protein attract macrophages to infiltrate in obese adipose tissue, ensuring chronic inflammation responses [68].

We performed our experimented on 3T3-L1 pre-adipocytes because 3T3-L1 pre-adipocytes are widely used *in vitro* model for white adipocytes differentiation, derived initially from Swiss mouse embryo tissue (mouse fibroblast line 3T3). When pre-adipocytes 3T3-L1 enter resting state; the rate of triglyceride synthesis increases significantly, which accumulates lipid drop inside cells to convert adipocyte cells [158]. Differentiated 3T3-L1 pre-adipocytes have a gene expression profile most similar

to white adipocytes; they also possess the characteristics of brown adipocytes in certain microenvironments but do not possess the characteristics of beige adipocytes [159]. The 3T3-L1 system has been pivotal in evolving the understanding of basic cellular mechanisms associated with obesity, diabetes, and related disorders. One of the limitations of this study is, *in vitro* modeling has lack of other organs that could influence insulin-resistant adipocytes. In vitro methods generally require the use of FBS, which limits several antibody uses.

Overall, Obese insulin resistance is associated with more than 20 types of clinical conditions. Demonstrating the pathophysiology of the obese insulin resistance associated clinical condition is hampered because we do not have a precise long-term obese insulin resistance model. To acknowledge the obese insulin resistance associated clinical conditions, our focus was on this obese insulin resistance model. We found that TNF-α and hypoxia inhibited insulin signaling and promoted pro-inflammation in a long-term manner on differentiated 3T3-L1 adipocytes. Therefore we assume that differentiated 3T3-L1 adipocytes develop an insulin resistance microenvironment because of TNF-α and hypoxia treatments. Despite our efforts to develop an obese insulin resistance *in vitro* model, further studies may require to confirm our model valid regarding *in vivo* obese insulin resistance conditions.

Chapter 4: High-fat Western diet and sugar water induced obesity contributes to increased PDX CRC tumor growth in Rag1 mice

4.1 Abstract

Because of Westernization, the obesity rate is increasing worldwide; if the current rate stays consistent, approximately half of the people will be obese by 2030. Epidemiological and experimental studies have demonstrated that obesity promotes colorectal cancer (CRC) tumor growth, but the exact mechanism is elusive. To further elucidation of the mechanism behind obesity-associated CRC requires new in vivo models. Our approach is to use an orthotopic implantation PDX animal model so that we can validate our in vitro 3D engineered PDX CRC platform for obesity-linked CRC studies. CRC tumor line 1101 (stage IV) was obtained from patients of Caucasian descent. To propagate the PDX line we used the SCID mouse subcutaneously xenograft model. Rag1 mice were divided into two groups, a high-fat diet with sugar water (HFS) group and a standard chow diet group with normal water, and were fed for 23 weeks. Mice were weighed twice a week. In the 13th week, PDX tumors isolated from SCID mice were implanted in the orthotopically in the cecum. In the 23rd week, mice were euthanized, and glucose and insulin were measured from blood samples. Epididymal white adipose tissue (EWAT) and tumors were excised and weighed. EWAT gene expression was analyzed using RT-qPCR The results showed that body weight, tumor weight, and EWAT significantly increased in the HFS diet mice compared to chow diet mice. Serum insulin levels and HOMA-IR score also significantly increased in the HFS group compared to the chow diet group mice. The gene expression study of EWAT showed that the pro-inflammatory genes *ccl2* and *TNF-α* significantly increased. On the other hand, the anti-inflammatory gene *adipoq* significantly decreased in EWAT. In conclusion, this study demonstrated that the same PDX line that was responsive *in vitro* was also responsive *in vivo*.

4.2 Introduction

Epidemiological studies indicate that diet-induced obesity and abdominal fat increased the risk of colorectal cancer (CRC). Currently, the high incidence areas for CRC worldwide are the United States, Europe, and Oceania [12]. It is believed that increasing adaptation of western life, including high consumption of saturated fat, simple sugars, and high-energy dense foods, may be the leading cause. Several studies have shown that obesity is associated with increased proliferation and decreased apoptosis of CRC tumor cells [16-18]. In the obese condition, adipose tissues secrete cytokines and growth factors, which results in a tumorigenic environment in the gastrointestinal tract that promotes CRC [15].

Moreover, increasing abdominal fat plays a pivotal role in the development of insulin resistance [160] by upregulating the cytokines (IL-1β, MCP-1, TNF-α, IL-6, etc.) leading to hyperinsulinemia, which develops into chronic low-grade inflammation. It has been demonstrated that obesity-induced IL-6 accelerates CRC tumor development by modulating the tumor microenvironment in a colitis-induced CRC model by macrophage polarization and successive lymphocyte recruitment [134]. However, risk of ulcerative colitis is not associated with obesity. Therefore, colitis-induced CRC carcinogenesis does not represent a good model of obesity-linked CRC [161].

Epidemiological and experimental studies have shown that there is a strong relationship between obesity and CRC, but the direct mechanism behind obesity-associated CRC is still elusive. An improved animal model may be required to unravel the underlying molecular mechanism responsible for obesity-linked CRC. Additionally, an appropriate animal model is need for the validation of our *in vitro* 3D engineered PDX CRC platform.

Our approach is to use an orthotopic implantation PDX animal model so that we can 1) examine the mechanism underlying the link between obesity and CRC and 2) validate our in vitro 3D engineered PDX CRC platform for obesity-linked CRC studies.

4.3 Methods

4.3.1 Reagents

Matrigel were from BD Biosciences, Inc (NJ, US). Chow diet was purchased from Teklad Global Rodent and High Fat Diet (HFD) was purchased from TestDiet ((5TJN; St Louis, MO, USA)). Dulbecco's modified Eagle's medium (DMEM), glutamine, and penicillin-streptomycin (P/S) were obtained from Gibco (Grand Island, NY, US). Trypsin/EDTA and HBSS were obtained from LONZA (Walkersville, MD, US). Fetal bovine serum (FBS) was from ATLANTA Biologicals (Lawrenceville, GA, US). SuperScript™ IV Reverse Transcriptase was purchased from Invitrogen (Lithuania). RNeasy Plus Micro and SYBR Green qPCR Mastermix kits were purchased from Qiagen (Valencia, CA, US). Isoflurane was obtained from Henry Schein (NY, US)

4.3.2 Animal study

Homozygous Rag1tm1Mom (Rag1) and SCID male mice (NOD-SCID gamma mouse) were obtained from Jackson Laboratory. The animals were housed in the College of Veterinary Medicine at Auburn University. All protocols for animal use and treatment were reviewed and approved by the Auburn University Animal Use and Care Committee. Mice were housed at 23°C with 50% humidity on a 12-h light/dark cycle and fed chow diet and water *ad libitum* for at least one week for acclimation.

4.3.3 Tumor growth subcutaneously

PDX CRC stage IV (1101) adenocarcinoma was isolated from a patient of Caucasian descent which was propagated subcutaneously in SCID mice. Approximately 5×10^6 frozen cells in sterile serum-free DMEM mixed 1:1 with sterile matrigel was injected subcutaneously on the flank immediately caudal to the axilla (detail protocol in appendix 1). The extent of tumor growth was monitored twice a week using Vernier calipers. Mice were euthanized by CO_2 asphyxiation followed by cervical dislocation prior to the tumor collection. Tumors were cut into $1mm^3$ cubes in DMEM media containing 1% P/S and kept on ice until implantation in Rag1 mice.

4.3.4 Tumor growth orthotopically

Rag1 mice at the age of seven weeks were divided into two groups and fed either a High fat diet with sugar water (HFS) (a 45% fat Western Diet with 42g/L fructose (55%) /sucrose (45%) in the drinking water) or a standard chow diet with normal water as control (Supplementary table 7.3). Two groups of mice were fed for 13 weeks and weight was measured twice a week. In the 13th week, mice were anesthetized with 2% isoflurane, the abdomen was shaved, a 1cm laparotomy was performed, the cecum was externalized, and a $1mm^3$ tumor was sutured to the colonic serosa using 8-0 nylon suture. The cecum was returned to its position in the abdomen, and the peritoneum was closed using 8-0 nylon suture, and the upper skin was stapled. Prior to being disconnected from anesthesia mice were injected with a pain killer according to their body weight. Mice were fed another ten weeks with HFS and chow diet. Tumor growth was graded twice a week by touching the abdomen using fingers.

4.3.5 Tissue collection and analysis

In the 23rd week, mice were fasted overnight, weighed and euthanized by CO_2 asphyxiation followed by decapitation. Trunk blood was collected, and blood glucose was measured by a Contour One blood glucose meter. Epididymal white adipose tissue (EWAT), liver, and heart were excised and weighed. Blood samples were centrifuged for 30min in full speed, serum was collected from the supernatant. Serum insulin levels were measured using insulin ELISA assay (Crystal Chem, Inc., Downers Grove, IL) and HOMA-IR was calculated using the formula (HOMA-IR = (26 * fasting serum insulin * fasting blood glucose) * 405). Collected blood serum, tumors, hearts, EWATs, and other organs were preserved in liquid nitrogen and then stored at -80°C.

4.3.6 RT-qPCR gene expression

Total RNA was extracted from the EWAT samples using RNeasy plus Micro kit. RNA was reversed transcribed using the SuperScript™ IV Reverse Transcriptase kit. Quantitative polymerase chain reaction (PCR) amplifications were performed using qPCR Mastermix. The following amplification conditions were used with 40 cycles of 15 seconds of denaturation at 95°C, followed by 1-minute annealing. Primers are shown in Table 4.1. Reactions were performed in triplicate, and data were calculated by the ΔΔCt method.

4.3.8 Statistical analysis

All experiments were run at least in triplicate. After checking for normal distribution, data were analyzed using either t-test or one way ANOVA with Tukey post-hoc test, depending upon the group of samples. P-values less than 0.05 ($P<0.05$) were determined to be a significant difference between groups.

Table 4.1 Quantitative PCR primers		
Genes		**Sequence (5′-3′)**
Ccl2 (MCP1)	Forward	caagatgatcccaatgagtag
	Reverse	ttggtgacaaaaactacagc
TNF-α	Forward	ctatgtctcagcctcttctc
	Reverse	catttgggaacttctcatcc
Adipoq (Adiponectin)	Forward	ccactttctcctcatttctg
	Reverse	ctagctcttcagttgtagtaac
IL6	Forward	aagaaatgatggatgctacc
	Reverse	gagtttctgtatctctctgaag
Eef2	Forward	agaacatatattgctggcg
	Reverse	caacagggttagatttcttg
GAPDH	Forward	
	Reverse	

4.4 Results

4.4.1 Rag1 mice fed HFS increased weight gain

To assess whether the HFS enhanced weight gain in Rag1 mice, the mice were weighed twice per week of the course of the experiment. Weight of HFS mice was greater than that of the chow diet fed mice at the 13th week when the PDX CRC tumors were implanted in the mice. (Fig 4.1) Bodyweight decreased in both dietary groups following surgery; however, bodyweight was recovered after few weeks of surgery. Prior to sacrifice at the 23rd week, the mice fasted overnight and the total bodyweight was measured, the data showed that bodyweight of HFS mice significantly (p=0.022) increased by 34.1 $\pm$ 1.8g (Fig 4.2) compared to chow diet mice. Tumor and EWAT were also measured, which were significantly (p-value 0.05 and 0.044 respectively) increased in the HFS group by 0.407 $\pm$ 0.32g and 1.32 $\pm$ 0.32g, respectively (fig 4.2) compared to chow diet mice
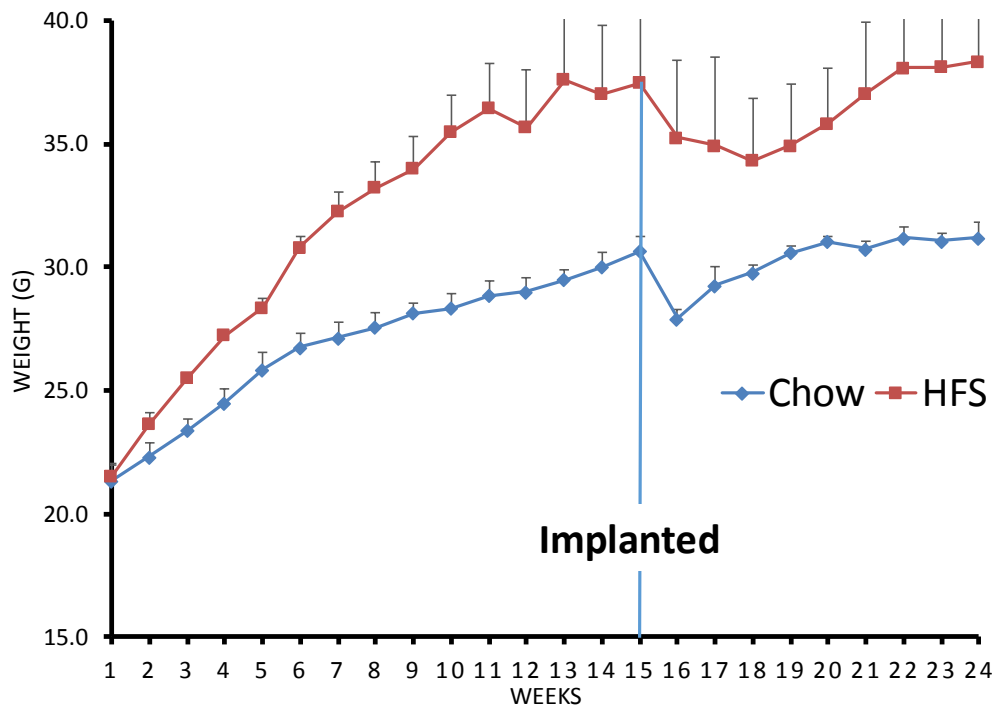
Fig 4.1: Weekly bodyweight of Rag1 mice fed HFS and chow diet: Two groups of mice fed HFS and chow diet for 23 weeks. In the 13th weeks, PDX tumors were implanted orthotopically and kept continued another ten weeks. Mice were sacrificed at 23rd weeks.
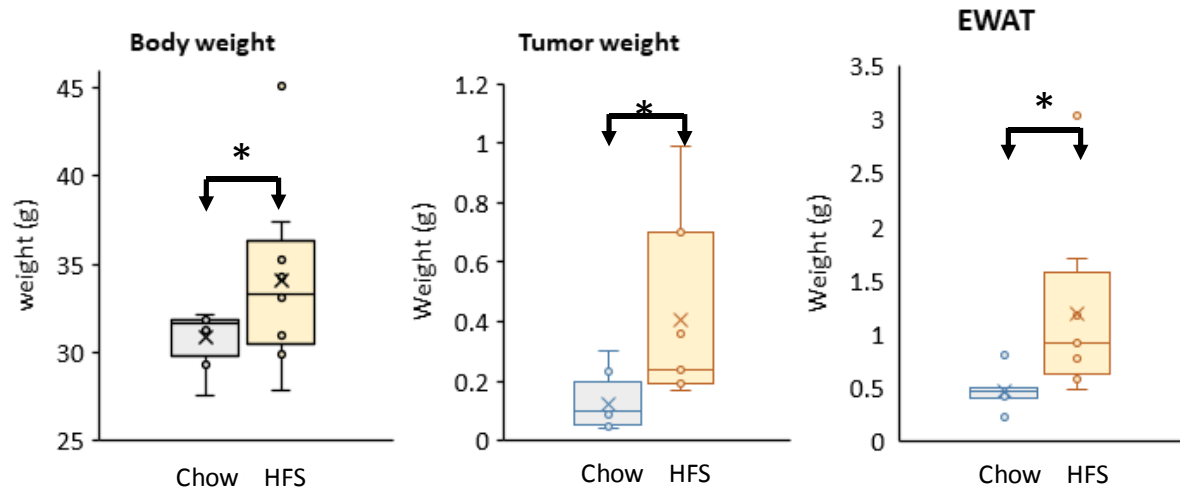
Fig 4.2: Final whole bodyweight, implanted tumor weight, and EWAT weight of Rag1 mice: Mice were sacrificed after 23 weeks. Whole-body weight, implanted tumor weight, and EWAT were measured in gram (g). Data are expressed with Box-Whisker plots with median, first (25th percentile) and third (75th) quartile range with minimum and maximum of the blot. Data were analyzed using the t-test. *p<0.05 was determined to be a significant difference between groups.

4.4.2 Rag1 mice fed HFS enhanced insulin resistance

To demonstrate the HFS-induced insulin resistance, several parameters were analyzed (4.2). The results showed that the serum insulin level in the HFS mice was significantly increased 100%. The HOMA-IR score was calculated from the serum insulin and blood glucose levels, and we found that the HOMA-IR significantly increased in HFS mice. To further confirm the insulin resistant state, we analyzed the EWAT tissue for markers of inflammation by gene expression study. The pro-inflammatory genes' *ccl2,* and *TNF-α* expressions significantly (p-value 0.048 and 0.009 respectively) increased by the fold changes 10.26 ± 0.46 and 3.14 ± 0.82 respectively (Fig: 4.3); on the other hand, the anti-inflammatory gene *adipoq* expression significantly (p=0.13) decreased by the fold change 0.72 ± 0.2.

Table 4.2: Bodyweight, liver weight, Glucose level, Insulin level, and HOMA-IR of Rag1 mice after 23 weeks		
	Chow	**HFS**
Serum Parameters		
Glucose (mg/dL)	207 ± 15	211 ± 23
Insulin (ng/mL)	0.44 ± 0.06	0.88 ± 0.16*
HOMA-IR	5.94 ± 0.96	12.80 ± 3.08*
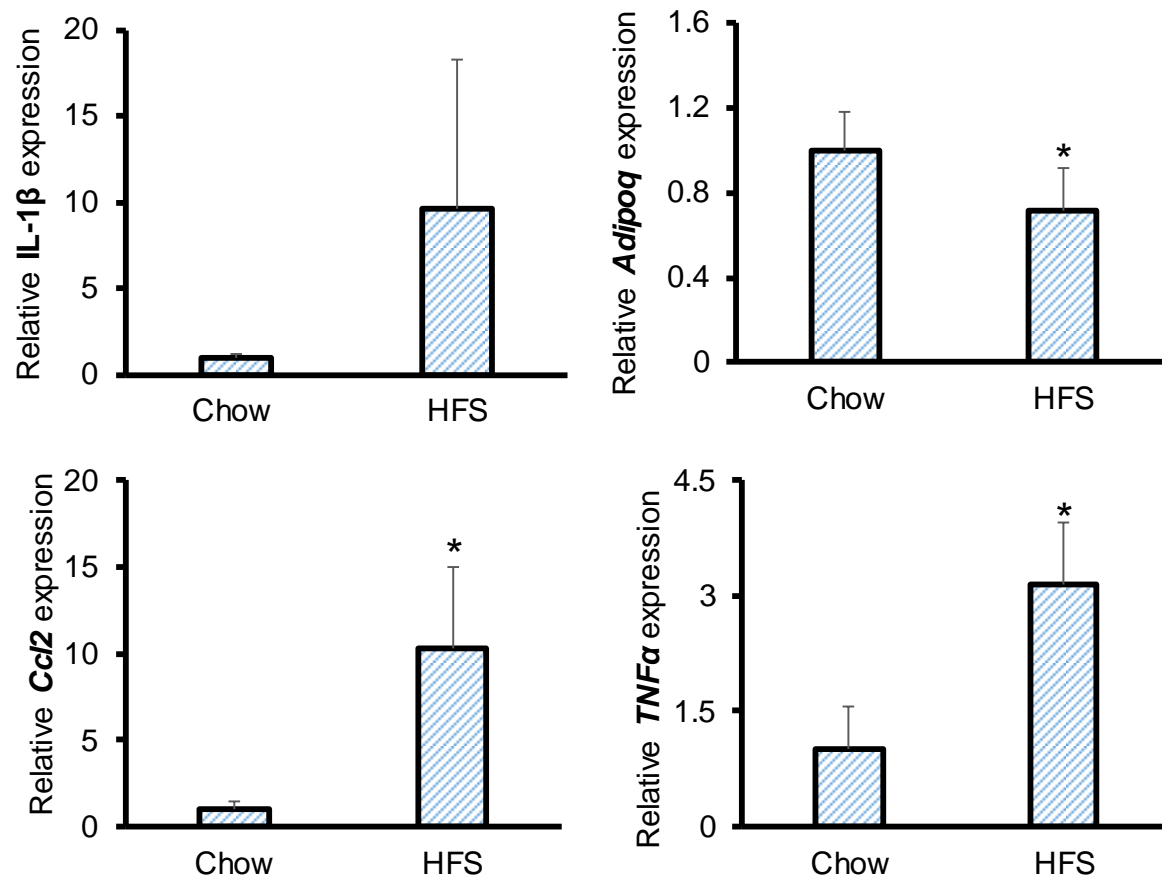
Fig 4.3: Inflammatory gene expression analysis of EWAT: EWAT was collected from tumor-bearing Rag1 mice fed HFS and chow diet for 23 weeks. *Ccl2, IL-1β, TNF-α*, and *adipoq* gene expression were analyzed using RT-qPCR. Gene expression was normalized using *B2M* and *GAPDH* as reference genes, and the ΔΔCt method was used to assess fold changes. Data were analyzed using the t-test. *p<0.05 was determined to be a significant difference between groups.

4.5 Discussion

The link between obesity and CRC is strong, but the detailed mechanism behind obesity-associated CRC is elusive. The study of connections has been hampered because of the lack of suitable models. A number of experimental studies that have been undertaken on diet-induced obesity-linked CRC, but none of these studies have used PDX CRC tumors implanted in an orthotopic manner in diet-induced obese mice to better model the heterogeneity of human tumors in the milieu of the obesity-modulated tumor microenvironment. Therefore, our aim was to implant PDX CRC tumors in diet-induced obese Rag1 mice to demonstrate the effect of obesity on human CRC tumors.

HFS significantly increased whole body and EWAT weight in the Rag1 mice, which confirmed that Rag1 mice are a good model of obesity for cancer studies [144]. To understand the insulin-resistant conditions, we analyzed the insulin level, HOMA-IR, and gene expression. The insulin level and HOMA-IR were significantly increased as were the expression of the pro-inflammatory genes *IL-6*, *TNF-α*, and *IL-1β*. On the other hand, the anti-inflammatory gene expression was significantly decreased. These results suggested that Rag1 mice developed insulin resistance *in vivo* in response to HFS feeding. Therefore, our data suggests that the obese insulin resistant state in Rag1 mice enhanced the PDX CRC tumor growth.

Rag1 mice have the mutated *Recombination-activating gene 1 (Rag1)* loci, which prevents mature T- and B-cell development. Their phenotype can be described as a "non-leaky" immune deficiency [162]. The protein encoded by the *Rag1* gene is involved in the recombination of signal sequences that flank the V, D and J regions in the genes that encode the heavy and light chain antibodies and the components of T-cell receptors. Complete loss of the function of the *rag1* gene, the main components responsible for

V(D)J recombination activity, is lost, which produces severe immunodeficiency [163]. However, these mice retained high levels of NK-cell activity and had limited engraftment [162].

Obesity alters secretion of hormones, and pro-inflammatory proteins which induces a low-grade inflammation. The obesity-associated metabolic micro-environment leads to induced cell proliferation, and reduced apoptosis, contributing to CRC [164, 165]. The progression of CRC has a positive correlation with insulin levels; insulin prompts cell proliferation and metastasis of CRC [166]. In the diet-induced obese mice, the production of pro-inflammatory chemokines and cytokines such as MCP-1 (*ccl2*), IL-1β, and TNF-α are increased in adipose tissue through the transcription factor NFkB which promotes insulin resistance [147-149] and eventually increase tumorigenesis [1]. Our data also showed that consumption of a HFD induced the production of *IL-6*, *IL-1β* and *TNF-α* in obese Rag1 mice; this result was associated with enhanced PDX tumor growth. Adiponectin increases energy expenditure and reduces adipocytes differentiation [151], which was also observed in our data. The effect of adiponectin was found to decrease in obese adipose tissue, and the deficiency is related to increased risk for obesity-related cancers [167]. Limitations of this study are Rag1 mice are immuno-deficient that cannot mimic the exact human tumor environment, and orthotopic surgery can cause significant pain or distress in mice.

Overall, this study concluded that Rag1 mice became obese and insulin resistant when consuming the HFS diet. Several inflammation-related parameters were altered in diet-induced obese Rag1 mice; these altered parameters may contribute to increased tumor growth in the obese orthotropic Rag1 model of human CRC.

Chapter 5: Development of an *in vitro* model of obesity-linked colorectal cancer using PDX 3D engineered PDX CRC tumors and insulin-resistant adipocytes

5.1 Abstract

Obesity is increasing alarmingly worldwide. Multiple studies demonstrated that there is a relationship between obesity and colorectal cancer (CRC). CRC is the costliest cancer and the five years survival rate is 65 percent. However, the detailed mechanism of obesity-linked CRC is elusive because of the lack of a relevant experimental models. Our approach is to establish a unique platform for culturing CRC tumors in an engineered PEG-Fb hydrogel. Patient-derived xenograft (PDX) CRC adenocarcinomas lines Stage II (1003), Stage III-B (1001) and Stage IV (1101) were obtained from male and female patients of Caucasian descent. Tumors were propagated in NOD-SCID gamma (SCID) mice subcutaneously and measured twice a week. PDX tumor cells were encapsulated in a PEG-Fb hydrogel and propagated for 29 days and determined the tumor growth rate. Our results showed that the growth phenotype of the 3D engineered CRC tissues followed that of the *in vivo* tumors. We determined the fastest growing line which was Stage II tumor (line 1003) to propagate in 2D and 3D culture for gene expression study. The gene expression analysis demonstrated that the *in vitro* 3D tumors were enabled to recapitulate the *in vivo* tumor characteristics. 3D engineered CRC tissue stage IV was co-cultured with long-term insulin resistance adipocytes. Most prominently, co-cultured with insulin resistance adipocytes enhanced the 3D engineered CRC tissue growth. In conclusion, it is demonstrated that 3D engineered PEG-Fb scaffold facilitated the 3D culture of CRC PDX tumors, and the insulin resistance 3T3-L1 differentiated adipocytes leads to enhanced 3D engineered CRC tissue growth.

5.2 Introduction

Currently, obesity is a major public health concern and the rate of obesity is increasing frighteningly. In the US, almost 40% of adults are considered to be obese [2]. Obesity contributes to several clinical conditions, including CRC. There is a strong link between obesity and CRC [6-8]. Many cytokines and growth factors released by adipose tissues have tumorigenic effects in the gastrointestinal tract, which promotes CRC [14]. It has been demonstrated that diet-induced obese mice develop insulin resistance and the pro-inflammatory environments that promote CRC [15]. CRC is the costliest type of cancer, the estimate indirect and direct cost is $ 17 billion by 2020 [10]. The understanding of the detailed mechanism of obesity-linked CRC and screening therapeutics has been hampered because relevant experimental models are lacking.

The conventional two-dimensional (2D) cell culture is severely restricted in its ability to imitate the *in vivo* tumor microenvironment. The drug testing of cancer in the conventional two-dimensional (2D) substrates is used for potential candidate drugs; however, the 2D culture system has failed to meet the desired levels of efficacy and safety in the clinical data [168]. In contrast, the tumor biopsy studies require direct patient access.. The most significant disadvantage of a biopsy study is that the amount of sample is limited; therefore, additional tests require additional samples. An alternative to the 2D model and the direct use of patient biopsies is the engineered cancer model which is generated by encapsulating tumor cells within three dimensional (3D) biomimetic scaffold. One of the widely tested scaffolds for 3D models is poly(ethylene glycol)-fibrinogen (PEG-Fb). The advantages of PEG-Fb is that it has the ability to form three dimensional (3D) engineered tissue; the mechanical properties, encapsulated cell types, and concentration can be readily modified; it is enabled to remodel and cells adhesion in the

hydrogel matrix in response to cell-secreted enzymes, and more significantly, PEG-Fb is known to be a secreted, deposited and influential factor in the tumorigenic behavior of cancer cells [169-172].

Our approach is to establish a unique platform for culturing PDX CRC cells in a 3D context using PEG-Fb, and to establish an *in vitro* obesity-linked CRC model using 3D engineered CRC tissues. In the first experiment, the growth, morphology, and transcriptional profile of 3D engineered CRC tissue in the PEG-Fb has been determined. In the second experiment, the 3D engineered CRC tissue has been co-cultured with our long-term obese insulin resistance model (the model is described in Chapter 3) to determine the growth, and morphology. Our preliminary data has shown that the growth and molecular characterization of 3D engineered CRC tissues mimic the *in vivo* PDX CRC tumors.

5.3 Methods

5.3.1 Reagents

Matrigel were from BD Biosciences, Inc (NJ, US). Collagenase IV and 100 U/mL DNase I were from Worthington biochemical corporation (NJ, US). Chow diet was purchased from Teklad Global Rodent. PEG-Fb was synthesized by Dr. Lipke lab (Department of Chemical Engineering, Auburn University, Auburn, AL). Poly-dimethyl siloxane (PDMS) was from Sigma-Aldrich (MO, US). Dulbecco's modified Eagle's medium (DMEM), glutamine, and penicillin-streptomycin (P/S) were obtained from Gibco (Grand Island, NY, US). Trypsin/EDTA and hanks' balanced salt solution (HBSS) were obtained from LONZA (Walkersville, MD, US). Fetal bovine serum (FBS) was from ATLANTA Biologicals (Lawrenceville, GA, US). SuperScript™ IV Reverse Transcriptase was from Invitrogen (Lithunia). RNeasy Plus Micro and SYBR Green qPCR Mastermix kits were purchased from Qiagen (Valencia, CA, US).

5.3.2 Animal study

The SCID mice (NOD.Cg-*Prkdc*[scid] Il2rg[tm1Wjl]/SzJ, Stock No: 005557) were obtained from Jackson Laboratory. The animals were housed in the College of Veterinary Medicine at Auburn University. All protocols for animal use and treatment were reviewed and approved by the Auburn University Animal Use and Care Committee. Mice were housed at 23°C and 50% humidity on a 12-h light/dark cycle and fed chow diet and water *ad libitum*. PDX CRC lines Stage II (line 1003), stage III-B (line 1001), and stage IV (line 1101) adenocarcinomas were isolated from male and female patients of Caucasian descent were propagated in SCID mice. Approximately 5 x 10^6 cells in sterile Serum-free DMEM mixed 1:1 with sterile Matrigel was injected subcutaneously on the flank immediately caudal to the axilla (Supplementary table 7.2). The extent of tumor growth was monitored twice a week by measuring length

(L) x wide (W) x height (H) using Vernier calipers. The LxWxH measurement was used to determine estimated tumor weight using the formula $v = 3.14/6$ (LxWxH). Mice were euthanized by CO_2 asphyxiation.

5.3.3 PDX CRC tumor cell dissociation

PDX CRC tumors were propagated subcutaneously in SCID mice. The fresh tumors were minced in small pieces in the dissociate solution. The dissociation solution was made by the mixture of Collagenase IV and DNase I and added 2ml per 1g of tissues. Samples were then incubated at 37 °C in a shaker for one hour, and total supernatant containing PDX CRC cells were strained in a 40μm strainer. The cell suspension was centrifuged, and the cell pellets were re-suspended in high glucose DMEM media with 10% FBS and 1% P/S. The process was done at least six times to remove dead cells and ECM debris. The viable cells were counted using a hem-cytometer.

5.3.4 3D engineered CRC tissue growth

Dissociated PDX CRC tumor cells (20 x 10^3 cell/ml) were suspended in the aqueous PEGFb polymer precursor solution. A platform of circular-shaped poly-dimethyl siloxane (PDMS) mold had 600μm thickness designed to encapsulate cells for making 3D engineered CRC tissue. A volume of 10 μL precursor solution was pipetted into the PDMS mold and exposed to the light with an intensity of 203 mW/cm^2 for 2 mins, which helped to make disc-shaped engineered 3D hydrogel. After 2min, the PDMS was peeled off and the hydrogel transferred to high glucose DMEM containing 10% FBS and 1% P/S media for tumor cell growth. Media were replaced every three days. The viability was assessed using live/dead staining, which was captured using a confocal microscope and quantified using ImageJ software (NIH). Cell growth was measured within the scaffolds by determining the cell density of the

3D engineered CRC tissue hydrogel. Dissociated PDX tumor cells were also seeded in 6-well plates for 2D culture and were provided high glucose DMEM containing 10% FBS and 1% P/S media; media were replaced every three days. 3D engineered CRC tissues were manufacture and propagated by Dr. Lipke lab (Department of Chemical Engineering, Auburn University, Auburn, AL)

5.3.5 RT-qPCR Gene Expression

Total RNA was extracted from the Stage II tumor samples propagated in SCID mice, 2D culture, and 3D culture using RNeasy plus Micro kit. RNA was reversed transcribed using the SuperScript™ IV Reverse Transcriptase kit. Quantitative polymerase chain reaction (PCR) amplifications were performed using qPCR Mastermix. The following amplification conditions were used with 40 cycles of 15 seconds of denaturation at 95°C, followed by 1-minute annealing. Prior to perform qPCR, primers were validated (Supplementary table 7.4). Primers are shown in Table 5.1, Reactions were performed in triplicate, and data were calculated by the $\Delta\Delta$Ct method.

Table 5.1 Quantitative PCR primers		
Genes		**Sequence (5′-3′)**
GPX2	Forward	aatttggacatcagaactgc
	Reverse	ggctgctcttcaagatttag
KDR	Forward	gtacatagttgtcgttgtagg
	Reverse	tcaatccccacatttagttc
SNAI1	Forward	ctctaatccagagtttaccttc
	Reverse	gacagagtcccagatgag
TGFβ1	Forward	aacccacaacgaaatctatg
	Reverse	cttttaacttgagcctcagc
LGR5	Forward	aaatgccttatgcttaccag
	Reverse	atcttgagcctgaaacattc
OLFM4	Forward	cccagttgttttccaatttc
	Reverse	cttctgagaaagaacatgagc
GAPDH	Forward	acagttgccatgtagacc
	Reverse	ttgagcacagggtacttta
B2M	Forward	gatcccacttaactatct
	Reverse	aaggactggtctttctat

5.3.6 Co-cultured 3D engineered CRC tissues with long-term insulin resistance adipocytes

PDX CRC tumors that were propagated subcutaneously in SCID mice derived from the stage IV was fabricated in the engineered 3D hydrogel. Engineered 3D hydrogels were co-cultured with long-term insulin resistance 3T3-L1 differentiated adipocytes; the process of insulin resistance modeling was described in Chapter 3. 3D engineered CRC tissues co-cultured with differentiated insulin-sensitive adipocytes were considered as control. Fresh insulin resistance and insulin sensitive adipocytes were supplied every three days for 8 days. Images were taken under a confocal microscope, and the intensity of cell growth was calculated using ImageJ software.

5.3.7 mRNA sequencing

Total RNA was extracted using the RNeasy Plus Micro Kit from the PDX tumors of SCID mice and 3D culture for the PDX lines. The quality and quantity of isolated RNA was measured using a Nano-drop (Thermo Scientific). RNA samples sent in dry ice to Hudson-alpha for RNA sequencing. The total RNA of these samples was evaluated for concentration by Qubit® and integrity was analyzed by 2100 Bioanalyzer at Hudson-alpha. Only samples with a RIN > 7 were selected for next-generation sequencing library preparation using MiSeq reagents of Illumina. MiSeq reagents enable up to 15 GB of output with 25 million sequencing reads and 2×300bp read lengths.

5.3.8 Statistical analysis

All experiments were run at least in triplicate. After checking for normal distribution, data were analyzed using either t-test or one way ANOVA with Tukey post-hoc test depends upon the group of samples. P-values less than 0.05 (P<0.05) was determined to be a significant difference between groups.

5.4 Results

5.4.1 Growth of the 3D engineered CRC tissues colony closely mimicked the *in vivo* tumor growth

To compare the growth of the three different human tumors in the 3D engineered CRC tissue from three different patients, tumors were propagated subcutaneously in SCID mice. We found that the growth rate of the three PDX tumors was different from each other (Fig 5.1). The fastest tumor was Stage II (Stage II), the average tumor growth for the fastest tumor was 0.384 gm/week (supplementary data fig 7.1), and the PDX tumor stage III-B had the lowest tumor growth rate. We also propagated the three lines of tumors in 3D engineered hydrogel for 29 days. The pattern of tumor growth of engineered tumors was almost similar to *in vitro tumors*. The highest slope value (681.85 $\mu m^2 x 10^4$/day) was found in the PDX line Stage II, and the lowest slope value was found in the PDX stage III-B (Fig 5.1).
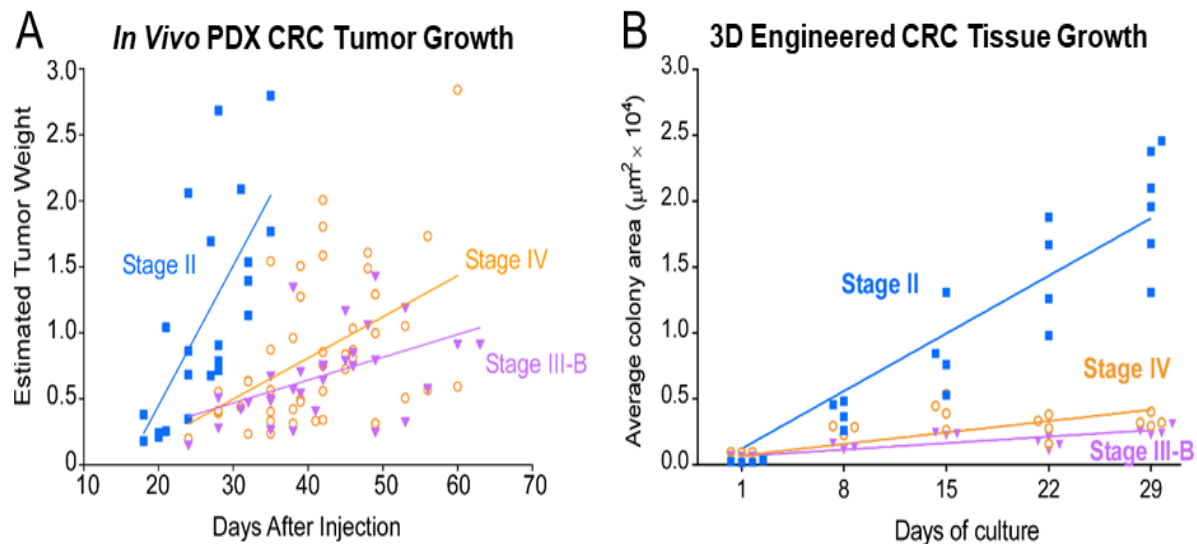
Fig 5.1: PDX tumor growth over time in SCID mice and engineered 3D tumors: Three PDX CRC lines from stage II (line 1003), stage III-B (line 1001), and stage IV (line 1101) were propagated in SCID mice. Tumor's growth was measured by Vernier calipers and calculated the volume by this formula v = 3.14/6 (LxWxH). The three PDX CRC lines were also propagated in the 3D engineered hydrogel for 29 days. Pictures were taken on days 8, 15, 22, and 29 under the microscope. Tumor cell viability was assessed. The growth of the tumor colony in the hydrogels was quantified using ImageJ software.

5.4.2 Gene expression of 3D engineered CRC tissues followed *in vivo* tumor characteristics

To examine gene expression of colon cancer markers of endothelial to mesenchymal transition (EMT), of stem cells, and angiogenesis, we performed RT-qPCR on total RNA isolated from PDX tumors grown in SCID mice, 3D engineered CRC tissues, and 2D cultured cells. The expression of the EMT markers *SNAI1* and *TWIST1*, which play a role for tumor metastasis, increased by a fold change of 8.15±0.71 and 4.91±0.66, respectively, in the 2D cultured cells compared to PDX tumors (p = 0.001 and p=0.005, respectively) (Fig 5.2A). In contrast, the expression of *TGFβ1* in both the 2D cultured cells and 3D engineered CRC tissues significantly increased by a fold change of 3.85±0.16 and 4.82±0.51, respectively, compared to PDX tumors (p=0.009 and p=0.003. respectively). However, no significant differences were found in the 3D engineered CRC tissues compared to PDX tumors. Next, we examined the expression of the stem cells marker genes *ALDH1A1*, *LGR5, GPX2,* and *OLFM4*. We observed a reduction in the expression of *ALDH1A1* (fold change 0.49±0.7), *LGR5* (fold change 0.43±0.11) and *OLFM4* (fold change 0.18±0.14) in the 2D cultured cells compared to the PDX tumor (p=0.016, p=0.022, and p=0.001, respectively) (Fig 5.2B). However, in the 3D engineered CRC tissues, *ALDH1A1* expression increased by fold change 1.61±0.17 (p=0.006) and *OLFM4* expression decreased by a fold change of 0.14±0.03 (p= 0.001) compared to the PDX tumors. No significant differences in the expression of *GPX2* were observed between the PDX tumors and the 2D cultured cells, and the 3D engineered CRC tissues. Lastly, we examined the expression of the angiogenesis marker genes *KDR* and *VEGFA* (Fig 5.2C). We observed that *KDR* expression increased by fold change 11.42±3.95 in the 2D cultured cells (p=0.028), and the *VEGFA* expression also increased but did not reach statistical significance. In contrast, the expression of *KDR* and *VEGFA* was similar between the 3D engineered CRC tissues and the PDX tumor. Taken together, our results on the expression of EMT, stem cell, and

angiogenesis markers suggested that gene expression is similar between the 3D engineered CRC tissues

and the PDX tumor but not between the 2D cultured cells and the PDX tumor.
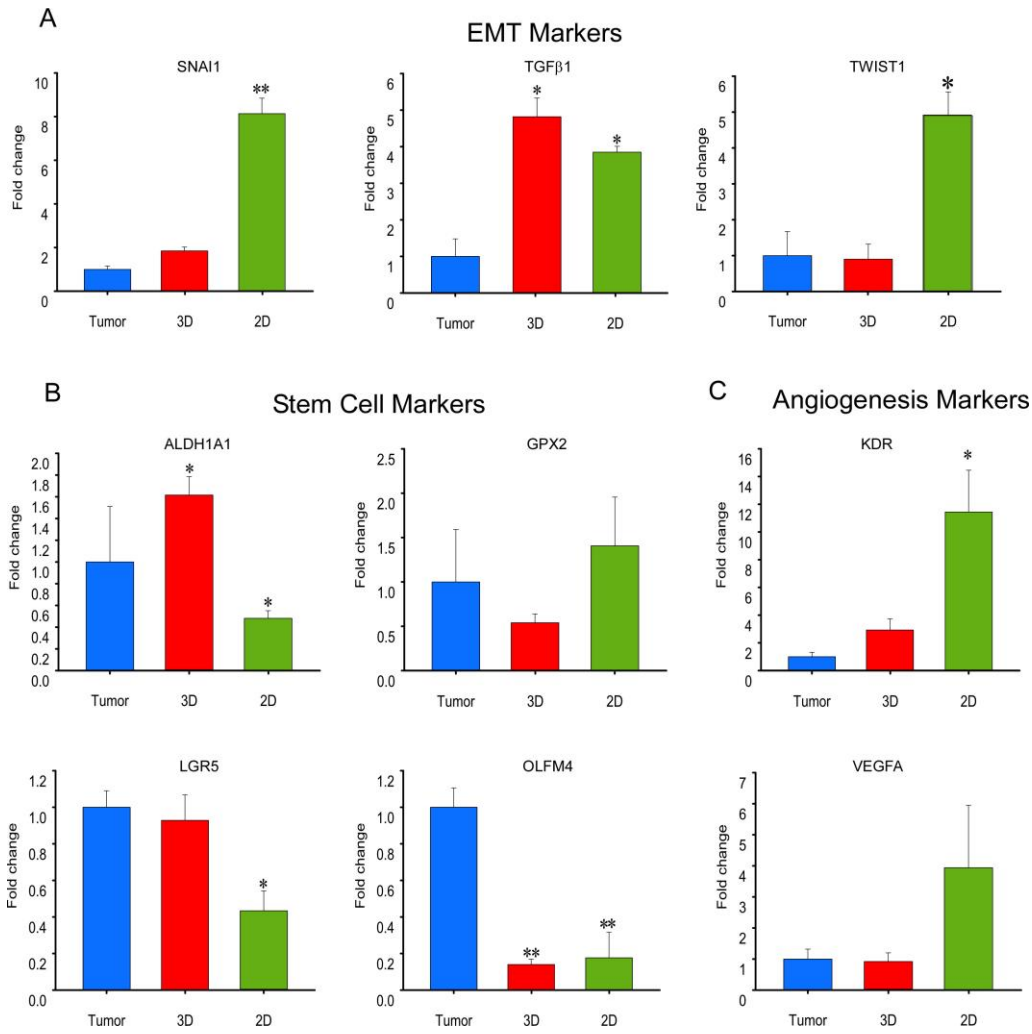
Fig 5.2: Gene expression of endothelial to mesenchymal transition, stem cell, and angiogenesis markers in PDX tumors grown in SCID mice, 3D engineered CRC tissue, and 2D cultured cells. RT-qPCR was performed using total RNA isolated from PDX CRC tumors propagated subcutaneously in SCID mice, 3D engineered CRC tissue, and 2D cultured cells. Gene expression was normalized using *B2M* and *GAPDH* as reference genes, and the $\Delta\Delta$Ct method was used to assess fold changes. Statistical significance was determined by one way ANOVA analysis followed by a Tukey post-hoc test. **A**. Endothelial to mesenchymal transition (EMT) markers: *TGFβ1*, *SNAI1*, and *TWIST1*. **B**. stem cell markers: *ALDH1A1*, *GPX2*, *LGR5*, and *OLFM4*. **C**. angiogenesis markers: *KDR* and *VEGFA* *$p<0.05$ and **$p<0.001$ compared to the PDX CRC tumors.

Day 1   Day 8

IR

IS

Scale bars=1000 μm, IR=Insulin
Resistant, IS=Insulin Sensitive
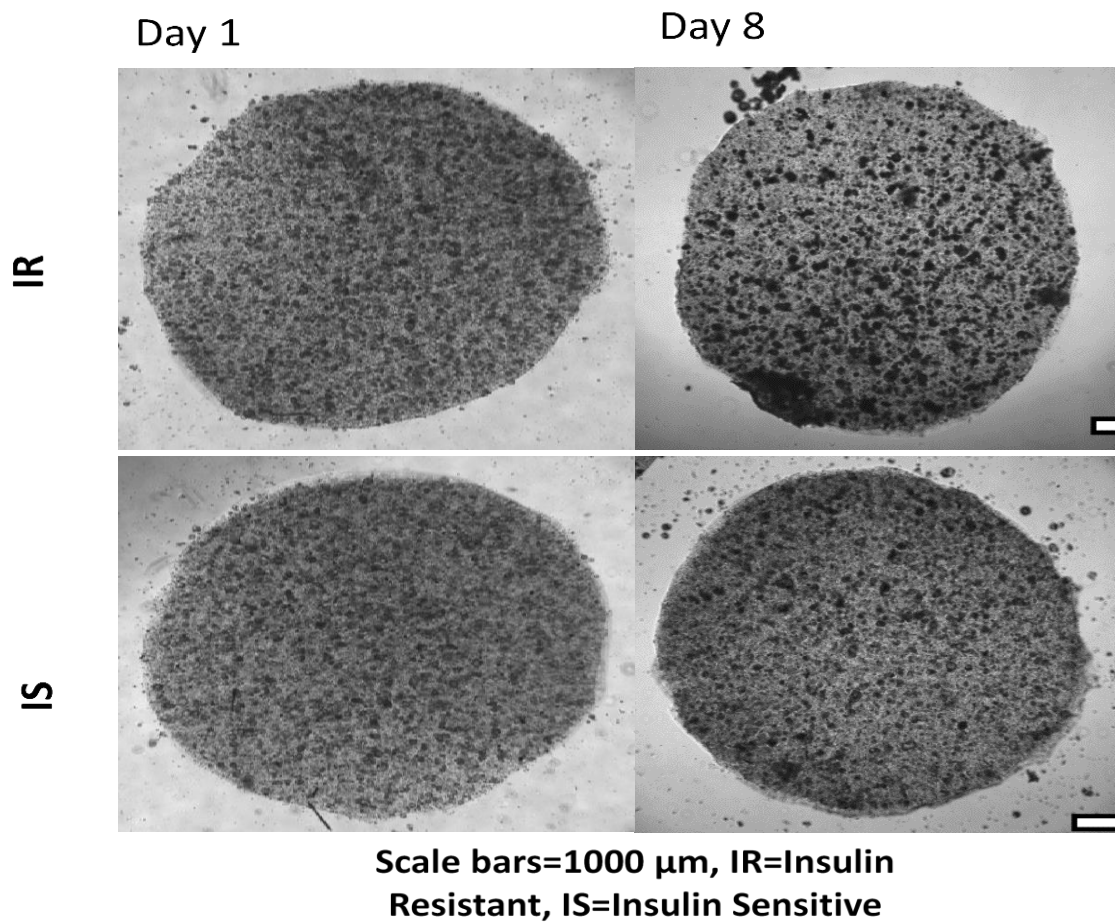
Fig 5.3: 3D engineered CRC tissues propagated with fresh Insulin resistance and Insulin sensitive adipocytes: 3D engineered CRC tissues co-cultured with long-term insulin resistance model for 8 days. Pictures were taken on days 8 and 8 under the microscope.

5.4.3 Insulin resistant 3T3-L1 differentiated adipocyte enhanced 3D engineered CRC tissue growth

To demonstrate the direct effect of the obese insulin resistance environment on 3D engineered tissue growth *in vitro*, we co-cultured the PDX stage IV with a long-term obese insulin resistance adipocyte model. We found that the tumor cell colony area in the hydrogels increased to greater extent when we co-cultured with insulin resistance differentiated adipocytes compared to the growth of the tumor cell colonies co-cultured with insulin-sensitive differentiated adipocytes (Fig 5.3). More cancer colonies (minuscule black dots) were observed in the 3D engineered CRC tissues co-cultured with insulin-resistant differentiated adipocytes over time. The graph (Fig 5.4) shows that the growth of the co-cultured cancer colony areas in the 3D hydrogels is significantly greater in the insulin-resistant microenvironment.
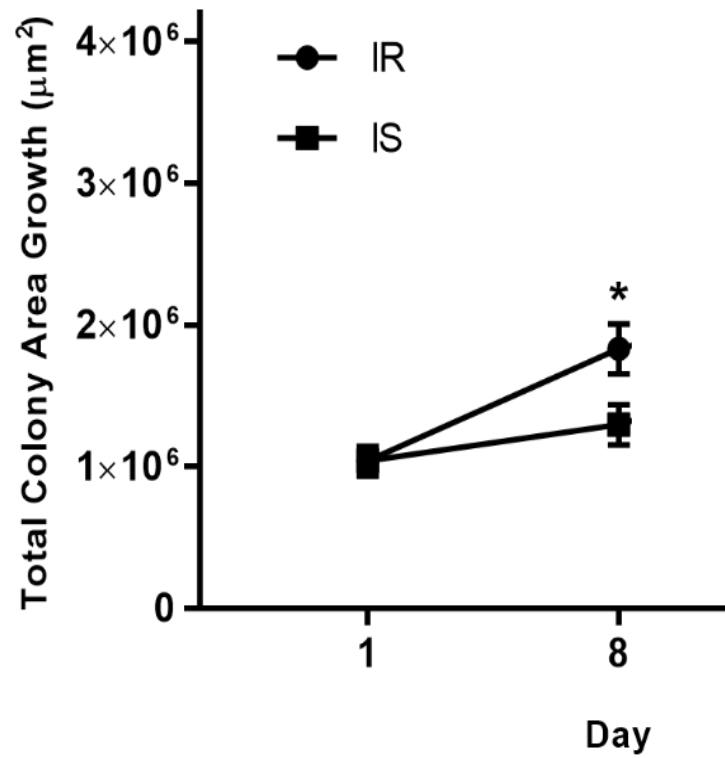
Fig 5.4: Growth of average colony area of 3D engineered CRC tissues co-cultured with insulin resistance and insulin sensitive adipocytes: 3D engineered CRC tissues co-cultured with long-term insulin resistance model for 8 days. Pictures were taken on days 1 and 8 under the microscope. Tumor cell viability was assessed. The growth of the tumor colony in the

5.4.4: Principle component analysis

Principle component analysis (PCA) demonstrated that 3D engineered CRC tissues (day 15) cluster with paired *in vivo* tumors were propagated in SCID mice for all three PDX CRC lines by bulk RNA seq transcriptomic analysis using HudsonAlpha Institute for Biotechnology's pipeline[173] with alignment to GRCh38 (Fig 5.5).
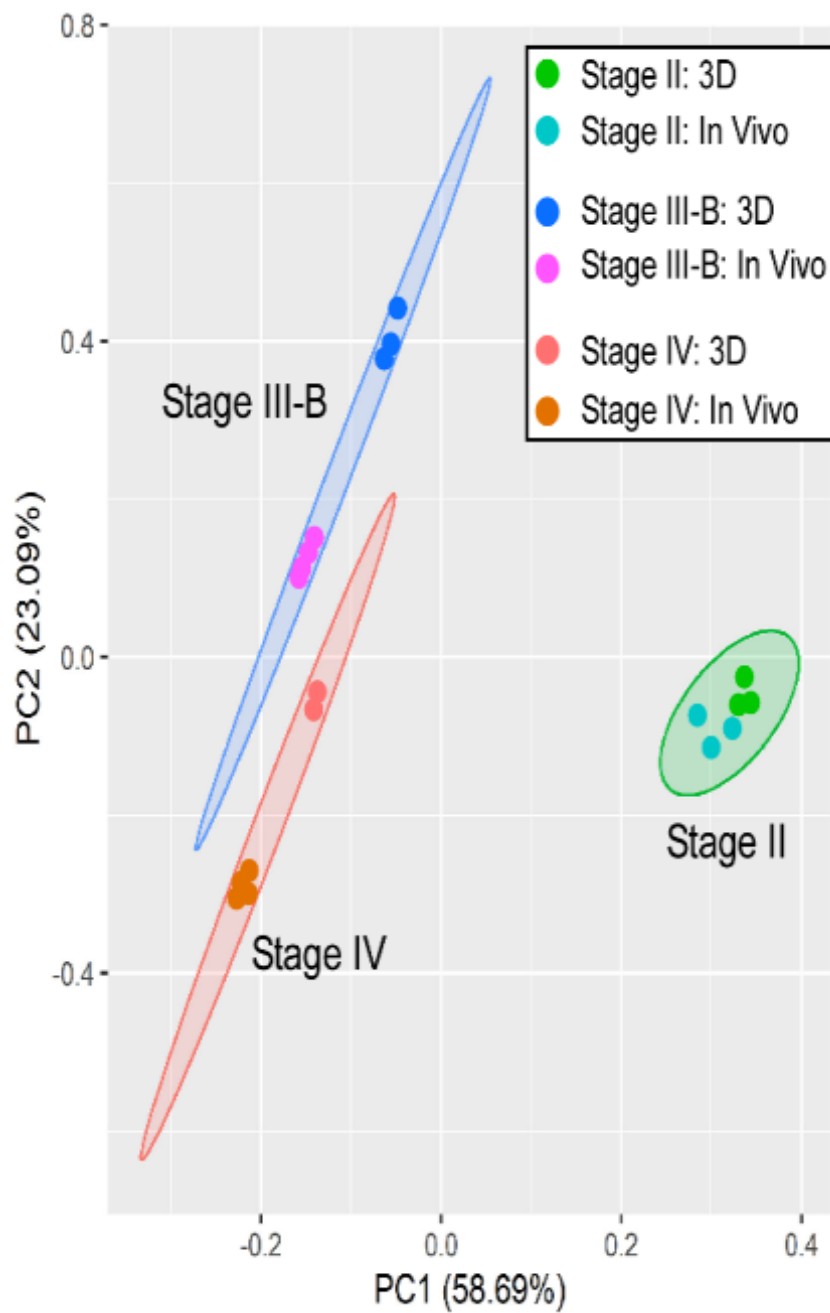
Fig. 5.5: Principle component analysis: Molecular analysis of 3D engineered tissues (3D) and *in vivo* tumors were propagated in SCID mice. PCA with K-means clustering using the top 300 discriminative genes in each PDX line. All samples originated from separately propagated tumors.

5.5 Discussion

The prevalence of obesity has risen but colon cancer death has been decreasing. However, there has been an increase in colon cancer deaths in the age groups under 50 [174]; this is thought to be due to the high prevalence of obesity. The complete understanding of the link between obesity-associated CRC and targeting new therapeutic agents are hampered because of the lack of proper models. It has been demonstrated that the conventional 2D and biopsy studies cannot fulfill the required criteria for bridging the gap for models to examine obesity-linked CRC. Therefore, we aimed to characterize 3D engineered CRC tissues by examining growth, morphology and gene expression; then the characterized 3D engineered CRC tissue were co-cultured with long-term insulin resistance 3T3-L1 differentiated adipocytes to examine the direct effect of obese insulin resistance via insulin resistant adipocytes on CRC tumor growth.

Three CRC tumors were collected from three different patients; the stages of the tumors were stage II (line 1003), stage III-B (line 1001), and stage IV (line 1101). These three types of tumors were propagated subcutaneously in SCID mice to determine the growth rate. We found the growth rate of these individual three tumors were different from each other. These three tumors also propagated in 3D culture encapsulated in PEF-Fb hydrogel; we found that the pattern of growth of each line in the 3D culture was almost similar to the *in vivo* tumor. We concluded that the 3D engineered CRC tissues model recapitulated *in vivo* tumor growth and micro-environment.

To further molecular characterization, we performed gene expressions study on PDX tumors, 3D engineered CRC tissues and 2D cultured cells. In this case, we chose three types of CRC markers; those were Epithelial to mesenchymal transition (EMT) markers, stem cell markers, and angiogenesis markers.

EMT is a cellular process in which cells lose their epithelial characteristics and gain mesenchymal properties. We examined the gene expression of three EMT markers *TGFβ1, SNAI1,* and *TWIST1*, which are associated with CRC, These genes play a pivotal role in CRC development by silencing E-cadherin expression, which prevents EMT [175-177]. During EMT, tumor cells acquire a mesenchymal phenotype that is responsible for cancer progression and metastasis activities [178]. We found that gene expression of all three EMT markers was increased significantly in 2D cultured cells compared to PDX tumors grown in SCID mice, while *TGFβ1* was the only marker also increased significantly in 3D engineered CRC tissues compared to the PDX tumors grown in SCID mice. The results suggest that these EMT markers are more metastatic in 2D culture. These results also suggest that EMT marker gene expression in 3D engineered CRC tissues are more similar to the PDX tumors grown in SCID mice than the 2D cultured cells. CRC stem cells are multipotent neoplastic cells that play a pivotal role in CRC tumor heterogeneity and tumor formation [179]. We examined the gene expression of four CRC stem cell markers *ALHH1A1*, *GPX2*, *LGR5*, and *OLFM4* [179-182]. The stem cell markers *ALDH1A1, LGR5, and OLFM4* are involved in cell proliferation and stem cell self-renewal by inducing transcription factor *c-Myc* [183-185] which is also known as a pro-oncogene, were significantly reduced in 2D cultured cells compared to PDX tumors grown in SCID mice, while *ALDH1A1* was increased and *OLFM4* was decreased in 3D engineered CRC tissues compared to the PDX tumors grown in SCID mice. *GPX2 is a ROS* scavenging enzyme, which is predominantly expressed by differentiated tumor cells in human colorectal tumor enriched cancer stem cells [180], we did not find any significant difference between the expressions of PDX tumors, 3D engineered CRC tissues, and 2D cultured cells. These results indicate that stem cell markers have shown more stemness in 3D culture. These results also indicate that CRC stem cell marker expression in 3D engineered CRC tissues are more similar to the PDX tumors grown in SCID mice than the 2D cultured cells. Angiogenesis is a critical step in cancer progression and

considered one of the hallmarks of cancer [186]. We examined the gene expression of two of the widely used angiogenesis markers, KDR, and VEGFA [187]. We did not observe any significant difference in gene expression between 3D engineered CRC tissues compared to the PDX tumors grown in SCID mice. Taken together, our results suggest that the 3D engineered CRC tissues were more similar in EMT, stem cell, and angiogenesis marker gene expression to the PDX tumors grown in SCID mice than the 2D cultured cells. A previous study has also demonstrated that the 3D PEG-Fb has the ability to recapitulate the heterogeneity that is inherent to native breast cancer tumors [172]. Based on these validations, our co-culture study was conducted. In this study, the fresh long-term insulin resistance 3T3-L1 differentiated adipocytes were supplied every three days until day 8 to co-culture with 3D engineered CRC tissues. The co-cultured experiment study demonstrated that insulin resistance micro-environment promoted engineered tumor growth significantly compared to insulin sensitive differentiated adipocytes. Several diet-induced obese mice have shown that the production of the pro-inflammatory chemokines and cytokines are increased in adipose tissue, which promotes insulin resistance [147-149] and eventually increases tumorigenesis [1, 18].

More than 100 types of matrices and scaffolds are being used currently for 3D culture; the most commonly used scaffolds are agarose, collagen, fibrinogen, and gelatin [188]. Scaffolds are used to synthesizing with synthetic hydrogels or some polymeric materials to generate the physical support for 3D cultures such as PEG poly(ethylene glycol), poly(vinyl alcohol, and 2-hydroxy ethyl methacrylate) [189]. The major advantage of 3D over 2D culture is; 3D cultures decrease in the gap between cell culture system and cellular physiology [190]. The 3D cultures are more novel and demonstrated in-depth insight into the mechanism by which tumor-derived cells function [191]. Our approach was to synthesize PEG-Fb (poly (ethylene glycol-fibrinogen) which was the combinations of fibrinogen (PF)

and poly (ethylene glycol) diacrylate (PEGDA). PEG-Fb was synthesized by Dr. Lipke's lab, Auburn University [172]. The advantage of PEG-Fb is that it has the ability to recapitulate the heterogeneity that is inherent to the native tumor over other traditional 3D tumors [172].

SCID mice have developed in the laboratory of Dr. Leonard Shultz at Jackson Laboratory is the most immune-deficient type of mice lacking mature T-cells, B-cells, macrophages, and natural killer cells [163]. SCID mice have a loss-of-function mutation in the mouse homologue of the human *prkdc* gene, which encodes a protein that resolves DNA strand breaks that occur during V(D)J recombination in developing T and B lymphocytes [192]. SCID mice also have a completed null *Il2rg* mutation in the gene encoding the interleukin 2 receptor gamma chain (IL2Rγ), absence of IL2Rγ blocks NK cell differentiation [193]. SCID mice are deficient in multiple cytokines signaling pathways and defects of innate immunity and allows engraftment of a wide range of primary tumor xenografts. SCID mice have the capacity of a high level of primary human tumor engraftment relative to other immune deficient mice [163]. Human tumor xenografts can preserve the tumor microenvironment during long-term engraftment in the SCID mice [194]. However, SCID mice have some disadvantages, such as these mice are lack of appropriate MHC molecules for T-cell selection in the thymus and low level of T-cell-dependent antibody responses [162].

Overall, this study focused on the PF based hydrogel for 3D culture by encapsulating PDX CRC tumors. A better model is certainly needed to understand the pathophysiology of obesity-associated CRC. In this case, our 3D hydrogel may serve as a standard platform for understanding the pathophysiology of obesity-linked CRC. In this case, the 3D engineered CRC tissues will facilitate similar cellular

physiology and characteristics like *an in vivo* tumor. To confirm our model, further experiment regarding

growth, morphology, and transcriptional characteristics may need to conduct.

Chapter 6: Summary and conclusion:

In this study, the following were undertaken: 1) TNF-α and hypoxia were used to developing a long-term obese insulin resistance model using 3T3-L1 differentiated adipocytes; 2) 3D engineered CRC tissues were characterized by growth, development, and gene expression; 3) The long-term obese insulin resistance adipocytes were co-cultured with the 3D engineered CRC tissues; and4) An orthotopic PDX CRC diet-induced obese animal model was investigated to demonstrate a standard *in vivo* platform for obesity-linked CRC study.

Overall, TNF-α and hypoxia successfully inhibited insulin signaling and promoted pro-inflammation in a long-term manner in differentiated 3T3-L1 adipocytes; this result provided us with a platform to modulate the tumor microenvironment *in vitro*. 3D engineered CRC tissues successfully modeled the growth and gene expression of PDX tumor propagated in SCID mice. Most remarkably, the 3D engineered CRC tissues co-cultured with the obese insulin-resistant model demonstrated that the obese insulin-resistant micro-environment promoted the 3D engineered CRC tissue growth, which was also observed in diet-induced obese Rag1 mice. The RNA sequencing data also has demonstrated that 3D engineered CRC tissues maintain similar gene expression to the tumors propagated in SCID mice. It is apparent that a better model is required to understand the pathophysiology of obesity-associated CRC. In this case, our 3D engineered hydrogels may serve as a standard platform for understanding the pathophysiology of obesity-linked diseases. Despite our efforts to develop an obese insulin resistance linked 3D model, further studies are required to confirm the validity of our model.

References:

1. Day, S.D., et al., *Linking inflammation to tumorigenesis in a mouse model of high-fat-diet-enhanced colon cancer.* Cytokine, 2013. **64**(1): p. 454-62.

2. Craig M. Hales, M.D., Margaret D. Carroll, M.S.P.H., Cheryl D. Fryar, M.S.P.H., and Cynthia L. Ogden, Ph.D., *Prevalence of Obesity Among Adults and Youth: United States, 2015–2016.* NCHS Data Brief October, 2017(288): p. 1-8.

3. Amadou, A., et al., *Overweight, obesity and risk of premenopausal breast cancer according to ethnicity: a systematic review and dose-response meta-analysis.* Obes Rev, 2013. **14**(8): p. 665-78.

4. Finkelstein, E.A., et al., *Obesity and severe obesity forecasts through 2030.* Am J Prev Med, 2012. **42**(6): p. 563-70.

5. Reaven, G.M., *The insulin resistance syndrome: definition and dietary approaches to treatment.* Annu Rev Nutr, 2005. **25**: p. 391-406.

6. Aleksandrova, K., et al., *Metabolic syndrome and risks of colon and rectal cancer: the European prospective investigation into cancer and nutrition study.* Cancer Prev Res (Phila), 2011. **4**(11): p. 1873-83.

7. Campbell, P.T., et al., *Impact of body mass index on survival after colorectal cancer diagnosis: the Cancer Prevention Study-II Nutrition Cohort.* J Clin Oncol, 2012. **30**(1): p. 42-52.

8. Renehan, A.G., et al., *Body-mass index and incidence of cancer: a systematic review and meta-analysis of prospective observational studies.* Lancet, 2008. **371**(9612): p. 569-78.

9. Ferlay, J., et al., *Cancer incidence and mortality worldwide: sources, methods and major patterns in GLOBOCAN 2012.* Int J Cancer, 2015. **136**(5): p. E359-86.

10. Mariotto, A.B., et al., *Projections of the cost of cancer care in the United States: 2010-2020.* Journal of the National Cancer Institute, 2011. **103**(2): p. 117-128.

11. Testa, U., E. Pelosi, and G. Castelli, *Colorectal cancer: genetic abnormalities, tumor progression, tumor heterogeneity, clonal evolution and tumor-initiating cells.* Med Sci (Basel), 2018. **6**(2).

12. Brenner, H., M. Kloor, and C.P. Pox, *Colorectal cancer.* Lancet, 2014. **383**(9927): p. 1490-1502.

13. Frezza, E.E., M.S. Wachtel, and M. Chiriva-Internati, *Influence of obesity on the risk of developing colon cancer.* Gut, 2006. **55**(2): p. 285-291.

14. Pathak, S., et al., *Obesity and colorectal liver metastases: Mechanisms and management.* Surg Oncol, 2016. **25**(3): p. 246-51.

15. Font-Burgada, J., B. Sun, and M. Karin, *Obesity and Cancer: The Oil that Feeds the Flame.* Cell Metab, 2016. **23**(1): p. 48-62.

16. Sikalidis, A.K., M.D. Fitch, and S.E. Fleming, *Diet induced obesity increases the risk of colonic tumorigenesis in mice.* Pathol Oncol Res, 2013. **19**(4): p. 657-66.

17. Tuominen, I., et al., *Diet-induced obesity promotes colon tumor development in azoxymethane-treated mice.* PLoS One, 2013. **8**(4): p. e60939.

18. Flores, M.B.S., et al., *RETRACTED: Obesity-induced increase in tumor necrosis factor-alpha leads to development of colon cancer in mice.* Gastroenterology, 2012. **143**(3): p. 741-753.e4.

19. Bluher, M., *Adipose tissue dysfunction in obesity.* Exp Clin Endocrinol Diabetes, 2009. **117**(6): p. 241-50.

20. Rigamonti, A., et al., *Rapid cellular turnover in adipose tissue.* PloS one, 2011. **6**(3): p. e17637-e17637.

21.   Sebo, Z.L. and M.S. Rodeheffer, *Assembling the adipose organ: adipocyte lineage segregation and adipogenesis in vivo.* Development, 2019. **146**(7).

22.   Lessard, J., et al., *Low abdominal subcutaneous preadipocyte adipogenesis is associated with visceral obesity, visceral adipocyte hypertrophy, and a dysmetabolic state.* Adipocyte, 2014. **3**(3): p. 197-205.

23.   Gustafson, B., et al., *Insulin resistance and impaired adipogenesis.* Trends Endocrinol Metab, 2015. **26**(4): p. 193-200.

24.   Osborn, O. and J.M. Olefsky, *The cellular and signaling networks linking the immune system and metabolism in disease.* Nat Med, 2012. **18**(3): p. 363-74.

25.   Bluher, M., *The distinction of metabolically 'healthy' from 'unhealthy' obese individuals.* Curr Opin Lipidol, 2010. **21**(1): p. 38-43.

26.   Eckel, N., et al., *Transition from metabolic healthy to unhealthy phenotypes and association with cardiovascular disease risk across BMI categories in 90 257 women (the Nurses' Health Study): 30 year follow-up from a prospective cohort study.* Lancet Diabetes Endocrinol, 2018. **6**(9): p. 714-724.

27.   Goossens, G.H., *The Metabolic Phenotype in Obesity: Fat Mass, Body Fat Distribution, and Adipose Tissue Function.* Obes Facts, 2017. **10**(3): p. 207-215.

28.   Pi-Sunyer, X., *The medical risks of obesity.* Postgrad Med, 2009. **121**(6): p. 21-33.

29.   Inoue, Y., et al., *Epidemiology of Obesity in Adults: Latest Trends.* Curr Obes Rep, 2018. **7**(4): p. 276-288.

30.   Morin, C.L., et al., *Adipose tissue-derived tumor necrosis factor-alpha activity is elevated in older rats.* J Gerontol A Biol Sci Med Sci, 1997. **52**(4): p. B190-5.

31.   Hales, C.M., et al., *Prevalence of Obesity Among Adults and Youth: United States, 2015-2016.* NCHS Data Brief, 2017(288): p. 1-8.

32.   Finkelstein, E.A., et al., *Annual medical spending attributable to obesity: payer-and service-specific estimates.* Health Aff (Millwood), 2009. **28**(5): p. w822-31.

33.   Mokdad, A.H., et al., *The spread of the obesity epidemic in the United States, 1991-1998.* Jama, 1999. **282**(16): p. 1519-22.

34.   *Vital signs: state-specific obesity prevalence among adults --- United States, 2009.* MMWR Morb Mortal Wkly Rep, 2010. **59**(30): p. 951-5.

35.   Gray, C.L., et al., *The association between physical inactivity and obesity is modified by five domains of environmental quality in U.S. adults: A cross-sectional study.* PloS one, 2018. **13**(8): p. e0203301-e0203301.

36.   Christakis, N.A. and J.H. Fowler, *The spread of obesity in a large social network over 32 years.* N Engl J Med, 2007. **357**(4): p. 370-9.

37.   Moellering, D.R. and D.L. Smith, Jr., *Ambient Temperature and Obesity.* Current obesity reports, 2012. **1**(1): p. 26-34.

38.   Hruby, A. and F.B. Hu, *The Epidemiology of Obesity: A Big Picture.* Pharmacoeconomics, 2015. **33**(7): p. 673-89.

39.   McKay, J.A. and J.C. Mathers, *Diet induced epigenetic changes and their implications for health.* Acta Physiol (Oxf), 2011. **202**(2): p. 103-18.

40.   Soubry, A., et al., *Obesity-related DNA methylation at imprinted genes in human sperm: Results from the TIEGER study.* Clin Epigenetics, 2016. **8**: p. 51.

41.   Speliotes, E.K., et al., *Association analyses of 249,796 individuals reveal 18 new loci associated with body mass index.* Nat Genet, 2010. **42**(11): p. 937-48.

42.   Villareal, D.T., et al., *Obesity in older adults: technical review and position statement of the American Society for Nutrition and NAASO, The Obesity Society.* Obes Res, 2005. **13**(11): p. 1849-63.

43.   Guo, S.S., et al., *Aging, body composition, and lifestyle: the Fels Longitudinal Study.* The American Journal of Clinical Nutrition, 1999. **70**(3): p. 405-411.

44.   Eveleth, P.B., et al., *Uses and interpretation of anthropometry in the elderly for the assessment of physical status. Report to the Nutrition Unit of the World Health Organization: the Expert Subcommittee on the Use and Interpretation of Anthropometry in the Elderly.* J Nutr Health Aging, 1998. **2**(1): p. 5-17.

45.   Gallagher, D., et al., *How useful is body mass index for comparison of body fatness across age, sex, and ethnic groups?* Am J Epidemiol, 1996. **143**(3): p. 228-39.

46.   Mozaffarian, D., et al., *Changes in diet and lifestyle and long-term weight gain in women and men.* The New England journal of medicine, 2011. **364**(25): p. 2392-2404.

47.   Al-Assal, K., et al., *Gut microbiota and obesity.* Clinical Nutrition Experimental, 2018. **20**: p. 60-64.

48.   Angelakis, E., et al., *The relationship between gut microbiota and weight gain in humans.* Future Microbiol, 2012. **7**(1): p. 91-109.

49.   Hollister, E.B., et al., *Structure and function of the healthy pre-adolescent pediatric gut microbiome.* Microbiome, 2015. **3**: p. 36.

50.   Meijnikman, A.S., et al., *Evaluating Causality of Gut Microbiota in Obesity and Diabetes in Humans.* Endocr Rev, 2018. **39**(2): p. 133-153.

51.   Stinson, L.F., et al., *The Not-so-Sterile Womb: Evidence That the Human Fetus Is Exposed to Bacteria Prior to Birth.* Frontiers in microbiology, 2019. **10**: p. 1124-1124.

52. Putignani, L., et al., *The human gut microbiota: a dynamic interplay with the host from birth to senescence settled during childhood.* Pediatr Res, 2014. **76**(1): p. 2-10.

53. Cotillard, A., et al., *Dietary intervention impact on gut microbial gene richness.* Nature, 2013. **500**(7464): p. 585-8.

54. Aron-Wisnewsky, J., J. Dore, and K. Clement, *The importance of the gut microbiota after bariatric surgery.* Nat Rev Gastroenterol Hepatol, 2012. **9**(10): p. 590-8.

55. Turnbaugh, P.J., *Microbes and Diet-Induced Obesity: Fast, Cheap, and Out of Control.* Cell host & microbe, 2017. **21**(3): p. 278-281.

56. Tremaroli, V., et al., *Roux-en-Y Gastric Bypass and Vertical Banded Gastroplasty Induce Long-Term Changes on the Human Gut Microbiome Contributing to Fat Mass Regulation.* Cell Metab, 2015. **22**(2): p. 228-38.

57. Liou, A.P., et al., *Conserved shifts in the gut microbiota due to gastric bypass reduce host weight and adiposity.* Sci Transl Med, 2013. **5**(178): p. 178ra41.

58. Turnbaugh, P.J., et al., *An obesity-associated gut microbiome with increased capacity for energy harvest.* Nature, 2006. **444**(7122): p. 1027-31.

59. Popkin, B.M., *The nutrition transition and obesity in the developing world.* J Nutr, 2001. **131**(3): p. 871s-873s.

60. Drewnowski, A., *Nutrition transition and global dietary trends.* Nutrition, 2000. **16**(7-8): p. 486-7.

61. Wadden, T.A., et al., *Lifestyle modification for obesity: new developments in diet, physical activity, and behavior therapy.* Circulation, 2012. **125**(9): p. 1157-70.

62. Moreno, L.A. and G. Rodriguez, *Dietary risk factors for development of childhood obesity.* Curr Opin Clin Nutr Metab Care, 2007. **10**(3): p. 336-41.

63.   Backus, R. and A. Wara, *Development of Obesity: Mechanisms and Physiology.* Vet Clin North Am Small Anim Pract, 2016. **46**(5): p. 773-84.

64.   Suganami, T., J. Nishida, and Y. Ogawa, *A paracrine loop between adipocytes and macrophages aggravates inflammatory changes: role of free fatty acids and tumor necrosis factor alpha.* Arterioscler Thromb Vasc Biol, 2005. **25**(10): p. 2062-8.

65.   Scott, T. and M.D. Owens, *Thrombocytes respond to lipopolysaccharide through Toll-like receptor-4, and MAP kinase and NF-kappaB pathways leading to expression of interleukin-6 and cyclooxygenase-2 with production of prostaglandin E2.* Mol Immunol, 2008. **45**(4): p. 1001-8.

66.   Cinti, S., et al., *Adipocyte death defines macrophage localization and function in adipose tissue of obese mice and humans.* J Lipid Res, 2005. **46**(11): p. 2347-55.

67.   Aouadi, M., et al., *Gene silencing in adipose tissue macrophages regulates whole-body metabolism in obese mice.* Proc Natl Acad Sci U S A, 2013. **110**(20): p. 8278-83.

68.   Weisberg, S.P., et al., *Obesity is associated with macrophage accumulation in adipose tissue.* J Clin Invest, 2003. **112**(12): p. 1796-808.

69.   Arner, E., et al., *Adipocyte turnover: relevance to human adipose tissue morphology.* Diabetes, 2010. **59**(1): p. 105-9.

70.   Maris, M., et al., *Deletion of C/EBP homologous protein (Chop) in C57Bl/6 mice dissociates obesity from insulin resistance.* Diabetologia, 2012. **55**(4): p. 1167-78.

71.   Manna, P. and S.K. Jain, *Obesity, Oxidative Stress, Adipose Tissue Dysfunction, and the Associated Health Risks: Causes and Therapeutic Strategies.* Metab Syndr Relat Disord, 2015. **13**(10): p. 423-44.

72.	Bakker, S.J., et al., *Cytosolic triglycerides and oxidative stress in central obesity: the missing link between excessive atherosclerosis, endothelial dysfunction, and beta-cell failure?* Atherosclerosis, 2000. **148**(1): p. 17-21.

73.	Furukawa, S., et al., *Increased oxidative stress in obesity and its impact on metabolic syndrome.* J Clin Invest, 2004. **114**(12): p. 1752-61.

74.	Basu, S., et al., *Conjugated linoleic acid induces lipid peroxidation in men with abdominal obesity.* Clin Sci (Lond), 2000. **99**(6): p. 511-6.

75.	Russell, A.P., et al., *Lipid peroxidation in skeletal muscle of obese as compared to endurance-trained humans: a case of good vs. bad lipids?* FEBS Lett, 2003. **551**(1-3): p. 104-6.

76.	Inoguchi, T., et al., *High glucose level and free fatty acid stimulate reactive oxygen species production through protein kinase C--dependent activation of NAD(P)H oxidase in cultured vascular cells.* Diabetes, 2000. **49**(11): p. 1939-45.

77.	Vincent, H.K., et al., *Mechanism for obesity-induced increase in myocardial lipid peroxidation.* Int J Obes Relat Metab Disord, 2001. **25**(3): p. 378-88.

78.	Qatanani, M. and M.A. Lazar, *Mechanisms of obesity-associated insulin resistance: many choices on the menu.* Genes Dev, 2007. **21**(12): p. 1443-55.

79.	de Mello, A.H., et al., *Mitochondrial dysfunction in obesity.* Life Sci, 2018. **192**: p. 26-32.

80.	Yin, X., et al., *Adipocyte mitochondrial function is reduced in human obesity independent of fat cell size.* J Clin Endocrinol Metab, 2014. **99**(2): p. E209-16.

81.	Heinonen, S., et al., *Impaired Mitochondrial Biogenesis in Adipose Tissue in Acquired Obesity.* Diabetes, 2015. **64**(9): p. 3135-45.

82.	Putti, R., et al., *Diet impact on mitochondrial bioenergetics and dynamics.* Front Physiol, 2015. **6**: p. 109.

83.   Zorzano, A., M. Liesa, and M. Palacin, *Role of mitochondrial dynamics proteins in the pathophysiology of obesity and type 2 diabetes.* Int J Biochem Cell Biol, 2009. **41**(10): p. 1846-54.

84.   Jheng, H.F., et al., *Mitochondrial fission contributes to mitochondrial dysfunction and insulin resistance in skeletal muscle.* Mol Cell Biol, 2012. **32**(2): p. 309-19.

85.   Hernandez-Aguilera, A., et al., *Mitochondrial dysfunction: a basic mechanism in inflammation-related non-communicable diseases and therapeutic opportunities.* Mediators Inflamm, 2013. **2013**: p. 135698.

86.   Rogge, M.M., *The role of impaired mitochondrial lipid oxidation in obesity.* Biol Res Nurs, 2009. **10**(4): p. 356-73.

87.   Muñoz, A. and M. Costa, *Nutritionally Mediated Oxidative Stress and Inflammation.* Oxidative Medicine and Cellular Longevity, 2013. **2013**: p. 1-11.

88.   Salvado, L., et al., *Targeting endoplasmic reticulum stress in insulin resistance.* Trends Endocrinol Metab, 2015. **26**(8): p. 438-48.

89.   Fu, S., et al., *Aberrant lipid metabolism disrupts calcium homeostasis causing liver endoplasmic reticulum stress in obesity.* Nature, 2011. **473**(7348): p. 528-31.

90.   Kawasaki, N., et al., *Obesity-induced endoplasmic reticulum stress causes chronic inflammation in adipose tissue.* Sci Rep, 2012. **2**: p. 799.

91.   Hotamisligil, G.S., *Endoplasmic reticulum stress and the inflammatory basis of metabolic disease.* Cell, 2010. **140**(6): p. 900-17.

92.   Zhang, Y., J.R. Sowers, and J. Ren, *Targeting autophagy in obesity: from pathophysiology to management.* Nat Rev Endocrinol, 2018. **14**(6): p. 356-376.

93.   Kim, K.H. and M.S. Lee, *Autophagy--a key player in cellular and body metabolism.* Nat Rev Endocrinol, 2014. **10**(6): p. 322-37.

94.   Lavallard, V.J., et al., *Autophagy, signaling and obesity.* Pharmacol Res, 2012. **66**(6): p. 513-25.

95.   Sinha, R.A., B.K. Singh, and P.M. Yen, *Reciprocal Crosstalk Between Autophagic and Endocrine Signaling in Metabolic Homeostasis.* Endocr Rev, 2017. **38**(1): p. 69-102.

96.   Cheng, Y., et al., *Therapeutic targeting of autophagy in disease: biology and pharmacology.* Pharmacol Rev, 2013. **65**(4): p. 1162-97.

97.   Blommaart, E.F., et al., *Phosphorylation of ribosomal protein S6 is inhibitory for autophagy in isolated rat hepatocytes.* J Biol Chem, 1995. **270**(5): p. 2320-6.

98.   Wang, K., *Molecular mechanism of hepatic steatosis: pathophysiological role of autophagy.* Expert Rev Mol Med, 2016. **18**: p. e14.

99.   Koga, H., S. Kaushik, and A.M. Cuervo, *Altered lipid content inhibits autophagic vesicular fusion.* FASEB J, 2010. **24**(8): p. 3052-65.

100.   Settembre, C., et al., *TFEB controls cellular lipid metabolism through a starvation-induced autoregulatory loop.* Nat Cell Biol, 2013. **15**(6): p. 647-58.

101.   Yang, L., et al., *Defective hepatic autophagy in obesity promotes ER stress and causes insulin resistance.* Cell Metab, 2010. **11**(6): p. 467-78.

102.   Qian, Q., et al., *S-Nitrosoglutathione Reductase Dysfunction Contributes to Obesity-Associated Hepatic Insulin Resistance via Regulating Autophagy.* Diabetes, 2018. **67**(2): p. 193-207.

103.   Singh, R., et al., *Autophagy regulates adipose mass and differentiation in mice.* J Clin Invest, 2009. **119**(11): p. 3329-39.

104.   Zhang, Y., et al., *Adipose-specific deletion of autophagy-related gene 7 (atg7) in mice reveals a role in adipogenesis.* Proc Natl Acad Sci U S A, 2009. **106**(47): p. 19860-5.

105.   Xia, Y., et al., *Enhanced infarct myocardium repair mediated by thermosensitive copolymer hydrogel-based stem cell transplantation.* Exp Biol Med (Maywood), 2015. **240**(5): p. 593-600.

106.   Cooper, G.M., *The cell: A Molecular Approach* ed. n. edition. 2000.

107.   Ganz, P.A., *Current US Cancer Statistics: Alarming trends in young adults?* J Natl Cancer Inst, 2019.

108.   Brown, C.C., *Toe temperature change: a measure of sleep onset?* Waking Sleeping, 1979. **3**(4): p. 353-9.

109.   Stratton, M.R., P.J. Campbell, and P.A. Futreal, *The cancer genome.* Nature, 2009. **458**(7239): p. 719-24.

110.   Todd, R. and D.T. Wong, *Oncogenes.* Anticancer Res, 1999. **19**(6A): p. 4729-46.

111.   Knudson, A.G., Jr., *Mutation and cancer: statistical study of retinoblastoma.* Proc Natl Acad Sci U S A, 1971. **68**(4): p. 820-3.

112.   Markowitz, S., *DNA repair defects inactivate tumor suppressor genes and induce hereditary and sporadic colon cancers.* J Clin Oncol, 2000. **18**(21 Suppl): p. 75S-80S.

113.   Arnold, M., et al., *Global patterns and trends in colorectal cancer incidence and mortality.* Gut, 2017. **66**(4): p. 683-691.

114.   Stracci, F., M. Zorzi, and G. Grazzini, *Colorectal cancer screening: tests, strategies, and perspectives.* Front Public Health, 2014. **2**: p. 210.

115.   Amin, M.B., et al., *The Eighth Edition AJCC Cancer Staging Manual: Continuing to build a bridge from a population-based to a more "personalized" approach to cancer staging.* CA Cancer J Clin, 2017. **67**(2): p. 93-99.

116.   Guinney, J., et al., *The consensus molecular subtypes of colorectal cancer.* Nat Med, 2015.
        21(11): p. 1350-6.

117.   CDC. *Cancers Associated with Overweight and Obesity Make up 40 percent of Cancers
        Diagnosed in the United States*. 2017; Available from:
        https://www.cdc.gov/media/releases/2017/p1003-vs-cancer-obesity.html.

118.   Ligibel, J.A., et al., *American Society of Clinical Oncology position statement on obesity and
        cancer.* J Clin Oncol, 2014. **32**(31): p. 3568-74.

119.   Arnold, M., et al., *Obesity and cancer: An update of the global impact.* Cancer Epidemiol,
        2016. **41**: p. 8-15.

120.   Sjostrom, L., et al., *Effects of bariatric surgery on cancer incidence in obese patients in Sweden
        (Swedish Obese Subjects Study): a prospective, controlled intervention trial.* Lancet Oncol,
        2009. **10**(7): p. 653-62.

121.   Shirakami, Y., et al., *Chemoprevention of colorectal cancer by targeting obesity-related
        metabolic abnormalities.* World J Gastroenterol, 2014. **20**(27): p. 8939-46.

122.   Joshi, R.K. and S.-A. Lee, *Obesity Related Adipokines and Colorectal Cancer: A Review and
        Meta-Analysis.* Asian Pacific Journal of Cancer Prevention, 2014. **15**(1): p. 397-405.

123.   Pietrzyk, L., et al., *Obesity and Obese-related Chronic Low-grade Inflammation in Promotion
        of Colorectal Cancer Development.* Asian Pacific Journal of Cancer Prevention, 2015. **16**(10):
        p. 4161-4168.

124.   Bjorge, T., et al., *Body mass index in adolescence in relation to cause-specific mortality: a
        follow-up of 230,000 Norwegian adolescents.* Am J Epidemiol, 2008. **168**(1): p. 30-7.

125.   Pendyala, S., et al., *Diet-induced weight loss reduces colorectal inflammation: implications for
        colorectal carcinogenesis.* Am J Clin Nutr, 2011. **93**(2): p. 234-42.

126. Bai, Y. and Q. Sun, *Macrophage recruitment in obese adipose tissue.* Obes Rev, 2015. **16**(2): p. 127-36.

127. Weisberg, S.P., et al., *Obesity is associated with macrophage accumulation in adipose tissue.* Journal of Clinical Investigation, 2003. **112**(12): p. 1796-1808.

128. Kratz, M., et al., *Metabolic dysfunction drives a mechanistically distinct proinflammatory phenotype in adipose tissue macrophages.* Cell Metab, 2014. **20**(4): p. 614-25.

129. Gordon, S., *Alternative activation of macrophages.* Nat Rev Immunol, 2003. **3**(1): p. 23-35.

130. Talmadge, J.E., M. Donkor, and E. Scholar, *Inflammatory cell infiltration of tumors: Jekyll or Hyde.* Cancer Metastasis Rev, 2007. **26**(3-4): p. 373-400.

131. Solinas, G., et al., *Tumor-associated macrophages (TAM) as major players of the cancer-related inflammation.* J Leukoc Biol, 2009. **86**(5): p. 1065-73.

132. Erreni, M., A. Mantovani, and P. Allavena, *Tumor-associated Macrophages (TAM) and Inflammation in Colorectal Cancer.* Cancer Microenviron, 2011. **4**(2): p. 141-54.

133. Geeraerts, X., et al., *Macrophage Metabolism As Therapeutic Target for Cancer, Atherosclerosis, and Obesity.* Front Immunol, 2017. **8**: p. 289.

134. Wunderlich, C.M., et al., *Obesity exacerbates colitis-associated cancer via IL-6-regulated macrophage polarisation and CCL-20/CCR-6-mediated lymphocyte recruitment.* Nat Commun, 2018. **9**(1): p. 1646.

135. Saijo, Y., et al., *Proinflammatory Cytokine IL-1 Promotes Tumor Growth of Lewis Lung Carcinoma by Induction of Angiogenic Factors: In Vivo Analysis of Tumor-Stromal Interaction.* The Journal of Immunology, 2002. **169**(1): p. 469-475.

136. Picon-Ruiz, M., et al., *Obesity and adverse breast cancer risk and outcome: Mechanistic insights and strategies for intervention.* CA Cancer J Clin, 2017. **67**(5): p. 378-397.

137. Williams, S.C., *Link between obesity and cancer.* Proc Natl Acad Sci U S A, 2013. **110**(22): p. 8753-4.

138. Gribovskaja-Rupp, I., L. Kosinski, and K.A. Ludwig, *Obesity and colorectal cancer.* Clin Colon Rectal Surg, 2011. **24**(4): p. 229-43.

139. Sheng, X., et al., *Adipocytes Sequester and Metabolize the Chemotherapeutic Daunorubicin.* Mol Cancer Res, 2017. **15**(12): p. 1704-1713.

140. Green, H. and O. Kehinde, *An established preadipose cell line and its differentiation in culture. II. Factors affecting the adipose conversion.* Cell, 1975. **5**(1): p. 19-27.

141. Lo, K.A., et al., *Analysis of in vitro insulin-resistance models and their physiological relevance to in vivo diet-induced adipose insulin resistance.* Cell Rep, 2013. **5**(1): p. 259-70.

142. Akash, M.S.H., K. Rehman, and A. Liaqat, *Tumor Necrosis Factor-Alpha: Role in Development of Insulin Resistance and Pathogenesis of Type 2 Diabetes Mellitus.* J Cell Biochem, 2018. **119**(1): p. 105-110.

143. Regazzetti, C., et al., *Hypoxia decreases insulin signaling pathways in adipocytes.* Diabetes, 2009. **58**(1): p. 95-103.

144. O'Neill, A.M., et al., *High-fat Western diet-induced obesity contributes to increased tumor growth in mouse models of human colon cancer.* Nutr Res, 2016. **36**(12): p. 1325-1334.

145. Bayascas, J.R. and D.R. Alessi, *Regulation of Akt/PKB Ser473 phosphorylation.* Mol Cell, 2005. **18**(2): p. 143-5.

146. Boucher, J., A. Kleinridders, and C.R. Kahn, *Insulin receptor signaling in normal and insulin-resistant states.* Cold Spring Harb Perspect Biol, 2014. **6**(1).

147. Arkan, M.C., et al., *IKK-beta links inflammation to obesity-induced insulin resistance.* Nat Med, 2005. **11**(2): p. 191-8.

148. Carlsen, H., et al., *Diet-induced obesity increases NF-kappaB signaling in reporter mice.* Genes & nutrition, 2009. **4**(3): p. 215-222.

149. Baker, R.G., M.S. Hayden, and S. Ghosh, *NF-kappaB, inflammation, and metabolic disease.* Cell Metab, 2011. **13**(1): p. 11-22.

150. Diez, J.J. and P. Iglesias, *The role of the novel adipocyte-derived hormone adiponectin in human disease.* Eur J Endocrinol, 2003. **148**(3): p. 293-300.

151. Bauche, I.B., et al., *Overexpression of adiponectin targeted to adipose tissue in transgenic mice: impaired adipocyte differentiation.* Endocrinology, 2007. **148**(4): p. 1539-49.

152. Halberg, N., et al., *Hypoxia-inducible factor 1alpha induces fibrosis and insulin resistance in white adipose tissue.* Mol Cell Biol, 2009. **29**(16): p. 4467-83.

153. Mazzatti, D., et al., *A microarray analysis of the hypoxia-induced modulation of gene expression in human adipocytes.* Arch Physiol Biochem, 2012. **118**(3): p. 112-20.

154. Yin, J., et al., *Role of hypoxia in obesity-induced disorders of glucose and lipid metabolism in adipose tissue.* Am J Physiol Endocrinol Metab, 2009. **296**(2): p. E333-42.

155. Ruan, H., et al., *Tumor necrosis factor-alpha suppresses adipocyte-specific genes and activates expression of preadipocyte genes in 3T3-L1 adipocytes: nuclear factor-kappaB activation by TNF-alpha is obligatory.* Diabetes, 2002. **51**(5): p. 1319-36.

156. Stephens, J.M., J. Lee, and P.F. Pilch, *Tumor necrosis factor-alpha-induced insulin resistance in 3T3-L1 adipocytes is accompanied by a loss of insulin receptor substrate-1 and GLUT4 expression without a loss of insulin receptor-mediated signal transduction.* J Biol Chem, 1997. **272**(2): p. 971-6.

157. Qi, C. and P.H. Pekala, *Tumor necrosis factor-alpha-induced insulin resistance in adipocytes.* Proc Soc Exp Biol Med, 2000. **223**(2): p. 128-35.

158.   Green, H. and M. Meuth, *An established pre-adipose cell line and its differentiation in culture.* Cell, 1974. **3**(2): p. 127-33.

159.   Morrison, S. and S.L. McGee, *3T3-L1 adipocytes display phenotypic characteristics of multiple adipocyte lineages.* Adipocyte, 2015. **4**(4): p. 295-302.

160.   Carey, D.G., et al., *Abdominal fat and insulin resistance in normal and overweight women: Direct measurements reveal a strong relationship in subjects at both low and high risk of NIDDM.* Diabetes, 1996. **45**(5): p. 633-8.

161.   Singh, S., et al., *Obesity in IBD: epidemiology, pathogenesis, disease course and treatment outcomes.* Nature reviews. Gastroenterology & hepatology, 2017. **14**(2): p. 110-121.

162.   Shultz, L.D., F. Ishikawa, and D.L. Greiner, *Humanized mice in translational biomedical research.* Nat Rev Immunol, 2007. **7**(2): p. 118-30.

163.   Hirenallur-Shanthappa, D.K., J.A. Ramírez, and B.M. Iritani, *Immunodeficient Mice*, in *Patient Derived Tumor Xenograft Models*. 2017. p. 57-73.

164.   Harvey, A.E., L.M. Lashinger, and S.D. Hursting, *The growing challenge of obesity and cancer: an inflammatory issue.* Ann N Y Acad Sci, 2011. **1229**: p. 45-52.

165.   Bardou, M., A.N. Barkun, and M. Martel, *Obesity and colorectal cancer.* Gut, 2013. **62**(6): p. 933-47.

166.   Chen, X., et al., *Insulin promotes progression of colon cancer by upregulation of ACAT1.* Lipids Health Dis, 2018. **17**(1): p. 122.

167.   Kelesidis, I., T. Kelesidis, and C.S. Mantzoros, *Adiponectin and cancer: a systematic review.* Br J Cancer, 2006. **94**(9): p. 1221-5.

168.   de Bono, J.S. and A. Ashworth, *Translating cancer research into targeted therapeutics.* Nature, 2010. **467**(7315): p. 543-9.

169. Rybarczyk, B.J. and P.J. Simpson-Haidaris, *Fibrinogen assembly, secretion, and deposition into extracellular matrix by MCF-7 human breast carcinoma cells.* Cancer Res, 2000. **60**(7): p. 2033-9.

170. LeBleu, V.S., B. Macdonald, and R. Kalluri, *Structure and function of basement membranes.* Exp Biol Med (Maywood), 2007. **232**(9): p. 1121-9.

171. Costantini, V., et al., *Fibrinogen deposition without thrombin generation in primary human breast cancer tissue.* Cancer Res, 1991. **51**(1): p. 349-53.

172. Pradhan, S., et al., *PEG-fibrinogen hydrogels for three-dimensional breast cancer cell culture.* J Biomed Mater Res A, 2017. **105**(1): p. 236-252.

173. Alonso, A., et al., *aRNApipe: a balanced, efficient and distributed pipeline for processing RNA-seq data in high-performance computing environments.* Bioinformatics, 2017. **33**(11): p. 1727-1729.

174. *American Cancer Society. Colorectal Cancer Facts & Figures 2017-2019.*
Atlanta: American Cancer Society; 2017.

175. Brzozowa, M., et al., *The role of Snail1 transcription factor in colorectal cancer progression and metastasis.* Contemporary oncology (Poznan, Poland), 2015. **19**(4): p. 265-270.

176. Xu, L., et al., *Activation of Wnt/beta-catenin signalling is required for TGF-beta/Smad2/3 signalling during myofibroblast proliferation.* J Cell Mol Med, 2017. **21**(8): p. 1545-1554.

177. Oh, B.Y., et al., *Twist1-induced epithelial-mesenchymal transition according to microsatellite instability status in colon cancer cells.* Oncotarget, 2016. **7**(35): p. 57066-57076.

178. Spaderna, S., et al., *A transient, EMT-linked loss of basement membranes indicates metastasis and poor survival in colorectal cancer.* Gastroenterology, 2006. **131**(3): p. 830-40.

179. Hatano, Y., et al., *Multifaceted Interpretation of Colon Cancer Stem Cells.* International journal of molecular sciences, 2017. **18**(7): p. 1446.

180. Emmink, B.L., et al., *GPx2 suppression of H2O2 stress links the formation of differentiated tumor mass to metastatic capacity in colorectal cancer.* Cancer Res, 2014. **74**(22): p. 6717-30.

181. Huang, E.H., et al., *Aldehyde dehydrogenase 1 is a marker for normal and malignant human colonic stem cells (SC) and tracks SC overpopulation during colon tumorigenesis.* Cancer research, 2009. **69**(8): p. 3382-3389.

182. Kemper, K., et al., *Monoclonal Antibodies Against Lgr5 Identify Human Colorectal Cancer Stem Cells.* STEM CELLS, 2012. **30**(11): p. 2378-2386.

183. Tomita, H., et al., *Aldehyde dehydrogenase 1A1 in stem cells and cancer.* Oncotarget, 2016. **7**(10): p. 11018-32.

184. Morgan, R.G., E. Mortensson, and A.C. Williams, *Targeting LGR5 in Colorectal Cancer: therapeutic gold or too plastic?* Br J Cancer, 2018. **118**(11): p. 1410-1418.

185. Liu, W. and G.P. Rodgers, *Olfactomedin 4 expression and functions in innate immunity, inflammation, and cancer.* Cancer Metastasis Rev, 2016. **35**(2): p. 201-12.

186. Hanahan, D. and R.A. Weinberg, *The hallmarks of cancer.* Cell, 2000. **100**(1): p. 57-70.

187. Mousa, L., M.E. Salem, and S. Mikhail, *Biomarkers of Angiogenesis in Colorectal Cancer.* Biomarkers in cancer, 2015. **7**(Suppl 1): p. 13-19.

188. Ravi, M., et al., *3D cell culture systems: advantages and applications.* J Cell Physiol, 2015. **230**(1): p. 16-26.

189. Fang, Y. and R.M. Eglen, *Three-Dimensional Cell Cultures in Drug Discovery and Development.* SLAS Discov, 2017. **22**(5): p. 456-472.

190.   Cukierman, E., et al., *Taking cell-matrix adhesions to the third dimension.* Science, 2001. **294**(5547): p. 1708-12.

191.   Muthuswamy, S.K., *3D culture reveals a signaling network.* Breast Cancer Res, 2011. **13**(1): p. 103.

192.   Blunt, T., et al., *Defective DNA-dependent protein kinase activity is linked to V(D)J recombination and DNA repair defects associated with the murine scid mutation.* Cell, 1995. **80**(5): p. 813-23.

193.   Shultz, L.D., et al., *Human lymphoid and myeloid cell development in NOD/LtSz-scid IL2R gamma null mice engrafted with mobilized human hemopoietic stem cells.* J Immunol, 2005. **174**(10): p. 6477-89.

194.   Simpson-Abelson, M.R., et al., *Long-term engraftment and expansion of tumor-derived memory T cells following the implantation of non-disrupted pieces of human lung tumor into NOD-scid IL2Rgamma(null) mice.* J Immunol, 2008. **180**(10): p. 7009-18.

Appendix 1:

Tumor growth rate (SCID mice)
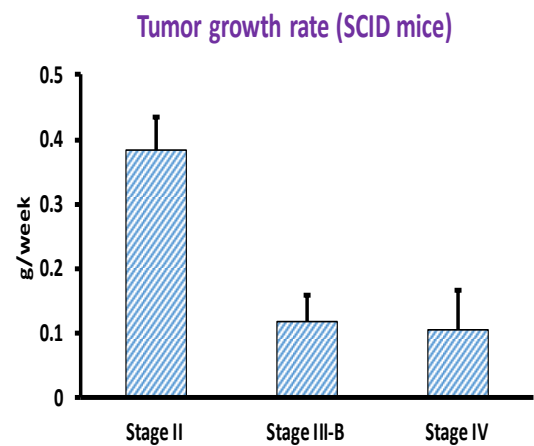
Supplementary data Fig 7.1: The approximate tumors growth rate gram per week

supplementary table 7.2: SCID mice study					
Animal	Strain	Passage	Sac date	Procedure	Procedure Date
4500	SCID	P4	8/30/2016	1001 P3 from 4498	7/8/2016
4501	SCID	P4	8/23/2016	1101 P3 from 4494	7/8/2016
4502	SCID	P3	9/12/2016	1001 + M P2	7/8/2016
4503	SCID	P3	8/12/2016	1003 + M P2	7/8/2016
4504	SCID	P3	9/6/2016	1101 + M P2	7/8/2016
4506	SCID	P4	9/6/2016	1001 P3 from 4499	7/19/2016
4507	SCID	P4	9/12/2016	1003 from 4503	8/12/2016
4508	SCID	P4	9/12/2016	1003 from 4503	8/12/2016
4509	SCID	P4	10/19/2016	1101 from 4504	9/6/2016
4510	SCID	P4	10/24/2016	1101 from 4504	9/6/2016
4511	SCID	P4	10/19/2016	1001 from 4502	9/12/2016
4512	SCID	P4	10/24/2016	1001 from 4502	9/12/2016
4584	SCID	P3	12/12/2016	1003 from M P2	11/4/2016
4585	SCID	P3	12/16/2016	1003 from M P2	11/4/2016
4576	SCID	P3	12/30/2016	1003 from M P2	11/21/2016
4580	SCID	P3	1/4/2017	1003 from M P2	11/23/2016
4581	SCID	P4	4/11/2017	1001 from M P3	12/7/2016
4582	SCID	P4	4/11/2017	1001 from M P3	12/7/2016
4583	SCID	P4	4/11/2017	1001 from M P3	12/7/2016
4592	SCID	P4	2/7/2017	1003 from 4585	12/16/2016
4598	SCID	P4	2/14/2017	1003 from 4576	12/30/2016
4599	SCID	P4	1/6/2017	1003 from 4576	12/30/2016
4577	SCID	P4	3/7/2017	1101 from M P3	2/2/2017
4578	SCID	P4	3/7/2017	1101 from M P3	2/2/2017
4579	SCID	P4	3/7/2017	1101 from M P3	2/2/2017
4612	SCID	p3	6/27/2017	1003 from m P2	5/19/2017
4613	SCID	p3	6/20/2017	1003 from m P2	5/19/2017
4614	SCID	p4	7/11/2017	1003 from m P3	6/16/2017
4615	SCID	p4	7/13/2017	1003 from m P3	6/16/2018
4616	SCID	p4	7/27/2017	1003 from m P3	6/30/2017
4617	SCID	p4	7/13/2017	1003 from m P3	6/30/2017
4618	SCID	P2	11/6/2017	1101 from m p1	9/12/2017
4619	SCID	P2	9/12/2017	1101 from m p1	9/12/2017
4620	SCID	P2	11/6/2017	1101 from m p1	9/12/2017
4661	SCID	p3	killed 2/15/17	1101 fresh from 4620	11/3/2017
4662	SCID	p4	12/26/2017	1101 from p3 m	11/17/2017
4663	SCID	p4	1/23/2018	1101 from p3 m	11/17/2017
4664	SCID	p4	12/12/2017	1003 from p3 M	11/14/2017
4665	SCID	p4	12/12/2017	1003 from p3 M	11/14/2017

Supplementary table 7.3: Rag1 mice study one					
Animal	Strain	Passage	Sac date	Procedure	Procedure Date
4586	Rag1	P5	5/10/2017	1101 implanted from 4577/4578/4579	3/7/2017
4587	Rag1	P5	5/10/2017	1101 implanted from 4577/4578/4579	3/7/2017
4588	Rag1	P5	5/10/2017	1101 implanted from 4577/4578/4579	3/7/2017
4589	Rag1	P5	5/10/2017	1101 implanted from 4577/4578/4579	3/7/2017
4590	Rag1	P5	5/10/2017	1101 implanted from 4577/4578/4579	3/7/2017
4591	Rag1	P5	5/10/2017	1101 implanted from 4577/4578/4579	3/7/2017
4592	Rag1	P5	3/8/2017	1101 implanted from 4577/4578/4579	3/7/2017
4593	Rag1	P5	3/8/2017	1101 implanted from 4577/4578/4579	3/7/2017
4594	Rag1	P5	3/8/2017	1101 implanted from 4577/4578/4579	3/7/2017
4595	Rag1	P5	5/10/2017	1101 implanted from 4577/4578/4579	3/7/2017
4596	Rag1	P5	3/10/2017	1101 implanted from 4577/4578/4579	3/7/2017
4597	Rag1	P5	3/8/2017	1101 implanted from 4577/4578/4579	3/7/2017
4598	Rag1	P5	5/10/2017	1101 implanted from 4577/4578/4579	3/7/2017
4599	Rag1	P5	died	1101 implanted from 4577/4578/4579	3/7/2017
4600	Rag1	P5	died	1101 implanted from 4577/4578/4579	3/7/2017
4601	Rag1	P5	5/10/2017	1101 implanted from 4577/4578/4579	3/7/2017
4602	Rag1	P5	5/10/2017	1101 implanted from 4577/4578/4579	3/7/2017
4603	Rag1	P5	5/5/2017	1101 implanted from 4577/4578/4579	3/7/2017
4604	Rag1	P5	5/10/2017	1101 implanted from 4577/4578/4579	3/7/2017
4605	Rag1	P5	5/10/2017	1101 implanted from 4577/4578/4579	3/7/2017
4606	Rag1	P5	3/8/2017	1101 implanted from 4577/4578/4579	3/7/2017
4607	Rag1	P5	3/8/2017	1101 implanted from 4577/4578/4579	3/7/2017
4608	Rag1	P5	5/10/2017	1101 implanted from 4577/4578/4579	3/7/2017
4609	Rag1	P5	5/10/2017	1101 implanted from 4577/4578/4579	3/7/2017
4610	Rag1	P5	5/10/2017	1101 implanted from 4577/4578/4579	3/7/2017
4611	Rag1	P5	5/10/2017	1101 implanted from 4577/4578/4579	3/7/2017
4612	Rag1	P5	3/8/2017	1101 implanted from 4577/4578/4579	3/7/2017

Supplementary Table 7.4: The RT-qPCR Ct (cycle threshold) values of the primers designed for human genes. The primer test was performed on the cDNA samples of PDX CRC tumors and mouse cell lines.

	PDX Tumor	PDX 2D	Mouse Control Cell Lines	
			3T3-L1[†]	MC38[‡]
EMT Markers				
SNAI1	35.2±0.5	35.1±0.0	36.3±0.2	37.2±0.7
TGFβ1	28.2±0.6	29.9±0.1	37.5±0.1	38.4±0.3
TWIST1	38.6±1.2	38.5±0.2	36.7±0.1	38.8±0.2
Stem Cell Markers				
ALDH1A1	32.1±10.9	35.2±0.6	35.8±0.3	35.8±0.5
GPX2	31.8±0.5	35.2±0.5	34.9±0.8	38.1±0.8
LGR5	28.6±0.2	34.6±0.7	37.2±0.2	41.4±1.5
OLFM4	33.6±1.1	41.7±0.9	37.6±0.7	42.7±0.2
Angiogenesis Markets				
KDR	34.2±0.2	37.4±0.3	34.5±0.2	36.5±0.5
VEGFA	31.1±0.2	32.5±0.5	35.9±0.0	36.9±0.2
Reference Genes				
GAPDH	23.6±0.6	28.7±0.4	36.5±0.6	36.9±0.6
B2M	26±0.5	29.1±0.43	37.9±0.9	37.3±0.5

[†] 3T3-L1, mouse fibroblast cell line

[‡] MC38, mouse colon cancer cell line

The protocol of thawing and injecting frozen PDX CRC tumor subcutaneously

❖ Thaw frozen cells rapidly (< 1 minute) in a 37°C water bath.

❖ Dilute the thawed cells using pre-warmed growth DMEM medium in a 5 ml tube. (It is recommended to use proper aseptic technique and work in a laminar flow hood)

❖ Centrifuge tumor cells in 5000 g for 5 min in room temperature

❖ Throw the supernatant and collect the pellet

❖ (Usually the tumor are chopped off and syringed using 16G-18G needle before freezing. If it is not, it is necessary to go through the process)

❖ For one vial of frozen cells add 250ul DMEM media and transfer to an Eppendorf tube

❖ And then add 250ul Matrigel, thaw the Matrigel in ice before adding to cells.

❖ Keep the mixture in ice until injected in mice

❖ Before injecting the tumor cells, keep the mouse in an asphyxiation chamber, take the mouse out from the chamber when the movement of the mouse becomes slow down

❖ Wipes the two flanks with 70% alcohol

❖ Inject 200ul mixture into the two flanks subcutaneously using an 18 gauge needle.